

Quantifying reworking and accumulation rates in a plaggic anthrosol using feldspar single-grain luminescence dating

MSC THESIS

ANNIKA VAN OORSCHOT

Supervisors: Tony Reimann and Jakob Wallinga

Chair group: Soil Geography and Landscape (SGL)

Student number: 940202623100

Submitted: March 2018

Abstract

Plaggic anthrosols are the soils resulting from fertilisation of arable land with a mixture of manure and plaggen sods cut from the rich organic Ah horizon of surrounding soils. During the Middle Ages, this self-sustaining type of agriculture was very productive. In the European sand belt, which covers parts of north-western Europe, Poland and the Baltic region, plaggic agriculture led to gradual accumulation of soil material and elevation of the soil surface. The rates of accumulation and of biological and anthropogenic soil reworking have not yet been clarified for plaggic soils while they might hold valuable information on historical agricultural practices in these soils. Such information will not only increase our understanding of historical agriculture, it might also help us improve future management of agricultural soils. The dual goal of this research is to provide insight in the history of a plaggic anthrosol and to test a newly developed feldspar single-grain luminescence dating protocol by Reimann et al. (2012). In this study the accumulation and reworking rates are calculated based on the ages of single grains of feldspar. A profile of a plaggic anthrosol near Denekamp in the east of the Netherlands was sampled. This location was selected because of the unique availability of recently determined, independent quartz OSL ages (Smeenge in preparation). The results indicate that plaggic agriculture at this location started around the beginning of the High Middle Ages (1000-1300 AD), which coincide with the Medieval Warm Period (950-1250 AD). This might suggest that the population growth and improved agricultural techniques in the High Middle Ages together with the improved climatic conditions of the Medieval Warm Period led to the cultivation of the sampled location for plaggic agriculture. High accumulation rates were found for a period extending far beyond the Middle Ages into the late 19th century. This leads to the conclusion that plaggic agriculture existed from the High Middle Ages until the late 19th century. Soil reworking was quantified by effective soil reworking rates rather than by the more commonly used apparent soil reworking rates. The effective soil reworking rate also accounts for the fraction of grains that do not participate in soil reworking. The effective soil reworking rates in the plaggic layers of the investigated plaggic anthrosol are one to two orders of magnitude larger than the reworking rates in the cover sand parent material, pointing out the difference between natural and anthropogenic soil mixing. The feldspar single-grain ages are all consistent with independent age estimates at the same location. An important advantage of dating single feldspar grains over dating single quartz grains is that a much larger percentage of the feldspar grains emits a suitable luminescence signal. This property combined with the consistency of the ages with independent age estimates from a well-established method and with the dates of historical events shows the potential of this new method for future applications.

Contents

Abstract	2
Introduction.....	5
Plaggic anthrosols	5
Luminescence dating of plaggic anthrosols	7
Research objectives.....	9
Background.....	10
Luminescence dating.....	10
Palaeodose	11
Dose rate	12
Measuring soil mixing using single-grain luminescence	13
Single-grain quartz dating	14
Single-grain feldspar dating.....	15
Analysis of single-grain distributions	16
Weighted mean age models.....	17
Minimum age model and maximum age model	17
Finite mixture model	17
Sampling location and site description	19
Experimental methods and details.....	20
Soil description and classification	20
Sampling.....	21
Measurements	21
Dose rate	21
Equivalent dose	22
Minimum age calculation	24
Minimum age model.....	25
Iterated weighted mean age.....	26
Selection of signal and age model.....	26
Soil reworking rates.....	29
Plaggen accumulation rates	31
Discussion and interpretation	33
Feldspar single-grain dating of plaggic soils in context.....	33
Start of plaggic agriculture	33
Natural and anthropogenic soil reworking	34

Historical accumulation of plaggen.....	35
Conclusions.....	38
Acknowledgements.....	39
References.....	40
Appendix.....	45
pIRIR sample descriptions.....	45
Radial plots.....	45
Equivalent dose distributions.....	47
IRSL sample descriptions.....	50
Radial plots.....	50
Equivalent dose distributions.....	52
Result tables.....	55
Overdispersion.....	55
Ages.....	55
Soil reworking rates.....	55
Plaggen accumulation rates.....	56

Introduction

Plaggic anthrosols

Plaggic anthrosols are the soils resulting from plaggic agriculture. This type of agriculture enabled continuous land use on one location, after hundreds of years of shifting cultivation (Giani et al. 2014). In this type of agriculture arable land was fertilised with organic material from the Ah horizon of surrounding soils. The plaggen sods were often cut from heathland and then brought to the stable as bedding. There they composted and became enriched with animal manure. Finally, they were spread out on the arable land as fertiliser (Dudal and Driessen 1991) (Figure 1). The thickness of the soil increases because the mineral fraction of the plaggen does not decompose. This type of agriculture is very labour intensive, so it was often applied on poor soils such as podzols (Blume and Leinweber 2004). Next to heather sods, grass sods were sometimes used. Their advantage was that they were better fertilisers (Pape 1970). However, grass sods competed with pasture land use (Niemeier and Taschenmacher 1939), so that heather plaggen were most commonly used. The area that was cut clear was usually much larger than the area on which the plaggen sods were applied. Estimates of the ratio of the application area to the clear-cut area range from 1:10 according to Niemeier and Taschenmacher (1939), Dudal and Driessen (1991) to 1:40 according to Behre (2000). Intensive cutting of heather sods resulted in land degradation and drift sand activity (Blume and Leinweber 2004). Mineral grains from these drift sands may have been brought to the plaggic soils by aeolian transport processes (Castel et al. 1989).

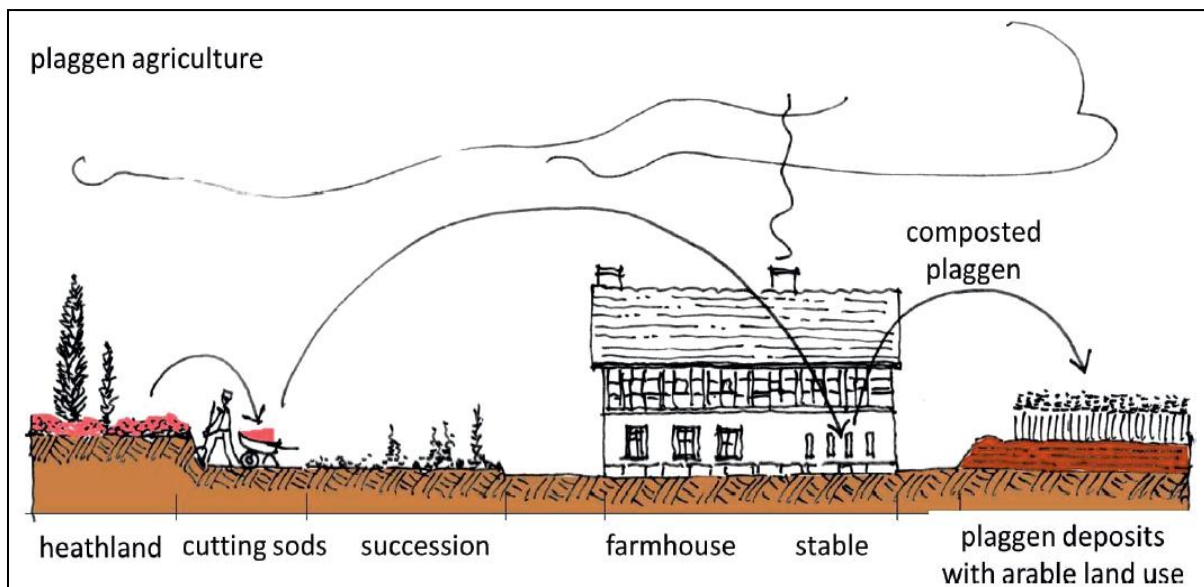


Figure 1 Method of plaggic agriculture. (Figure from Giani et al. (2014), drawn by Klaus Thierer)

Blume and Leinweber (2004) conclude from a literature survey that plaggic agriculture in Northwest Europe seems to have started on the islands of Sylt and Föhr in the North Sea and later spread to Germany and the Netherlands. The parent material of these areas is mostly Pleistocene cover sand in which nutrient-poor soils developed. This is probably the reason why plaggic agriculture became popular (Giani et al. 2014). The vertically striped area in Figure 2 is now worldwide the largest area in which plaggic anthrosols occur discontinuously and it covers an area of around 0.5 million ha (Dudal and Driessen 1991).

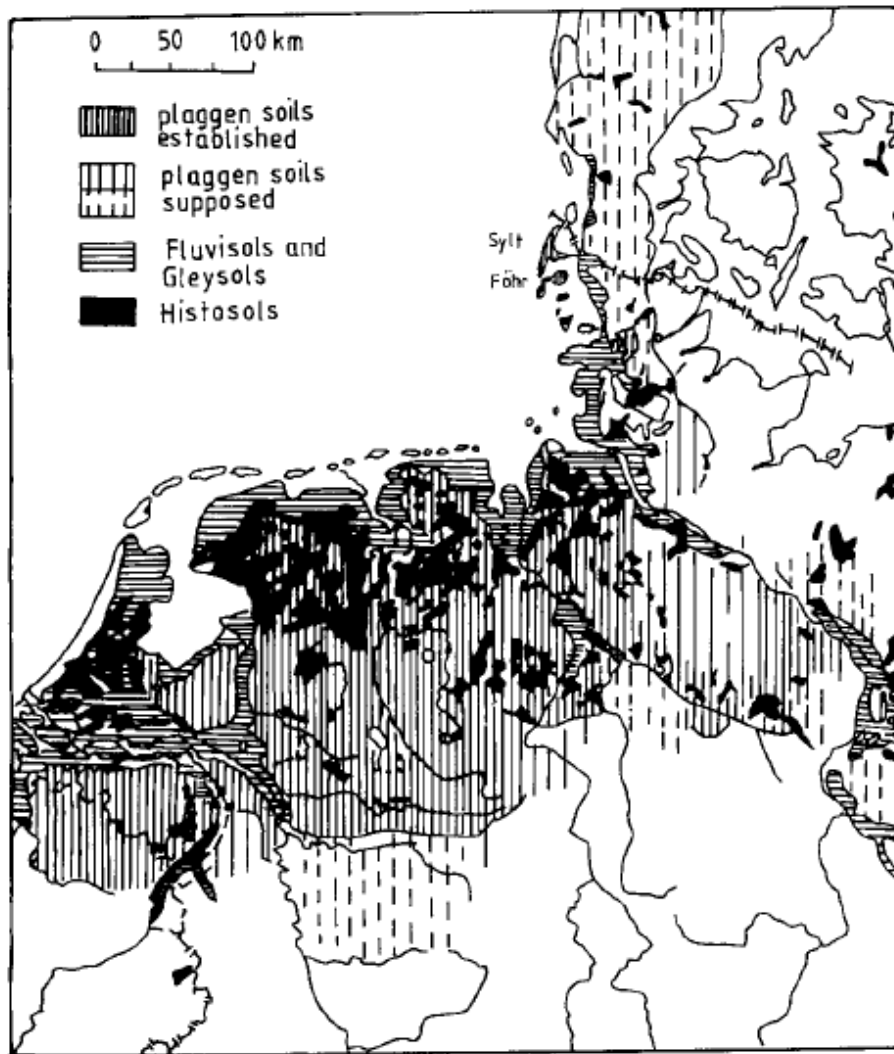


Figure 2 Established and supposed plaggenic soils (all vertically striped areas) in northwest Europe. In the indicated areas plaggenic soils do not occur continuously. Figure from Blume and Leinweber (2004), original figure from Niemeier and Taschenmacher (1939).

Plaggenic agriculture started about 1000 years ago according to radiocarbon dating studies, but estimates vary between 600 AD and 1100 AD (e. g. Fastabend and von Raupach 1962, Heineman 1973). The invention of artificial fertilisers around the beginning of the twentieth century marked the end of plaggenic agriculture (Spek 2004). The use of artificial fertilisers has increased dramatically since that time. Application of artificial fertilisers increased yields and it was less labour intensive than the plaggenic system. However, due to the high productivity of this modern type of agriculture the soil is depleted of nutrients, so it needs a constant input of new fertiliser. One of the main components of artificial fertiliser is phosphorus. Phosphorus is derived from rock, which is a non-renewable source. While phosphorus demand is still increasing, the sources of phosphorus are estimated to be depleted in 50 to 100 years (Cordell et al. 2009). This stresses the need for a self-sustaining agricultural system that does not depend on finite external (i.e. not locally available) resources. Plaggenic agriculture is an early example of a sustainable agricultural system for food production. As mentioned earlier, it has existed for centuries without loss of productivity. It would be interesting to explore the possibilities of this type of agriculture for modern applications. However, it should be kept in mind that the productivity of plaggenic agriculture is low compared to the productivity of modern agriculture and that the carrying

capacity of the landscape for plaggic agriculture is limited. At the peak time of plaggic agriculture in northwest Europe the population density and thus the area needed for food production was much smaller than it is now, but even during that time the carrying capacity of the landscape was sometimes exceeded, resulting in drift sand activity on the locations where sods were removed from the soil (Lungershausen et al. 2017). Using the 1:10 ratio mentioned by Niemeier and Taschenmacher (1939), there will simply not be enough land to sustain plaggic agriculture for the present-time food demand. It is therefore not an option to go back to these old agricultural practices, but still there might be much we can learn from this former type of agriculture that was fully self-sustaining and productive over a prolonged period of time. Another advantageous property of plaggic soils is that they are extremely rich in stable organic matter, so their potential for carbon sequestration (e.g. Freibauer et al. 2004, Merante et al. 2017) could be large. If we could return to agricultural soils that contain more organic matter, more organic carbon is incorporated in the soil, possibly contributing to a lower carbon dioxide level in the atmosphere. Therefore, it is important to have a proper idea of how plaggic soils were managed. Examples of such management aspects are the soil reworking rate resulting from bioturbation and ploughing and the accumulation rate, which is the rate of elevation of the soil surface level due to application of plaggen sods.

The rates of accumulation and soil reworking can be derived from ages at several depths in the soil. In the past, efforts have been made to date plaggic anthrosols using radiocarbon dating (Van Mourik et al. 1995). A problem of this method is that the ages of carbon found in a sample do not necessarily reflect the age of deposition. Some of the organic material in the soil may be formed in situ, while other organic material has originated from the sods that were applied as manure (Bokhorst et al. 2005). The origin of pollen in a sample is also uncertain. They may have been inside the applied sods as well (Mucher et al. 1989). For these reasons, radiocarbon dating and palynological dating will not give reliable accumulation and mixing rates. Luminescence dating does not provide the formation age of soil material, but it dates the time since mineral grains were last exposed to daylight. This makes it possible to determine the mixing rates and accumulation rates.

Luminescence dating of plaggic anthrosols

The long and rich history of plaggic agriculture can be unravelled using luminescence dating. Using this dating method, the age of mineral soil material can be derived from the radiation dose that the grain has received from its surroundings during burial (called burial dose, estimated by the palaeodose). This will be explained in detail in the background section. In contrast to laboratory experiments, which usually do not last for more than a few years, luminescence dating can provide insight into the long-term effects of land management on soil properties. The conventional multiple grain quartz optically stimulated luminescence (OSL) method has already been used to date plaggic anthrosols (e. g. Bokhorst et al. 2005, Van Mourik et al. 2011, Van Mourik et al. 2012). They used the single aliquot regenerative dose (SAR) technique to determine the palaeodose and the age of the samples. Bokhorst et al. (2005) found that the aliquot size was too large to determine if the luminescence signal of individual grains was zeroed during aeolian deposition or because of ploughing activities that transported the grain to the surface. Therefore Bokhorst et al. (2005) proposed analysis of smaller aliquots to separate these two processes. Small-aliquot SAR has already been used by Van Mourik et al. (2011) to determine the ages of a mineral soil matrix. They compared these ages to the radiocarbon ages of the same sample and proved that the organic material in the spaces between mineral grains was older than the mineral matrix.

Using conventional multiple grain quartz OSL measurements, the moment that the luminescence signal started to accumulate in a grain can be dated reliably and it represents the moment that the grain was buried below the ploughing layer. In addition, single-grain analysis potentially provides extra information on soil processes occurring over time, such as mixing and accumulation rates. These rates could contain information on former land use methods. For example, the reworking rate as a result of ploughing could be derived from the dose distributions of the grains in the ploughing horizon. It is expected that this rate was low in the early Middle Ages, so ploughing horizons of that age will contain relatively old grains that have never surfaced due to the low ploughing intensity. When the ploughing intensity started to increase, more grains reached the surface and thus the dose distributions of more intensively ploughed layers are expected to be narrower. The moment at which plaggen sods started to be added to the soil should also be visible from the dose distributions, because the addition of sods to the soil results in a rise of the soil surface and therefore also of the lower boundary of the ploughing horizon. Single-grain measurements are labour intensive and time consuming and only a few percent of the quartz grains emit a luminescence signal that is bright enough for measurement. On the other hand, several tens of percent of the feldspar grains are suitable for luminescence dating (Reimann et al. 2012), which is an order of magnitude more than for quartz. Because many feldspar grains give a suitable signal, the feldspar mineral is especially useful for single grain measurements. Although most soil samples will contain more quartz than feldspar, measurement of the feldspar signal is more efficient than measurement of the quartz signal.

Research objectives

This study has two objectives. On the one hand, it assesses how the feldspar single-grain dating protocol as developed by Reimann et al. (2012) performs in determining the accumulation and reworking rates in plaggic soils. In addition, these rates will be used to clarify the history of these soils. This knowledge may be applied in modern agriculture to create healthy soils containing more stable organic matter and thereby making agricultural practices more sustainable.

The accumulation and reworking rates contain much information on historical plaggic agriculture. The effective reworking rate is defined by the speed at which the soil is reworked (sample depth divided by apparent luminescence burial age) and the number of grains that participate in reworking (Reimann et al. 2017). The accumulation rate is the speed at which the soil surface elevates because of plaggic addition. Spek (2004) expresses the need for a detailed and statistically reliable dating method for determining the ages of layers in a plaggic anthrosol to get a better impression of the accumulation rate over time. He also states that detecting and dating vertical displacement of soil material requires analysis of the age distribution of a large dataset rather than dating individual soil elements. Single-grain dating provides such age distributions and feldspar is the most efficient mineral to use. For these reasons the feldspar single-grain luminescence dating method will be used in this study.

The first appearance of plaggic agriculture is not well established yet because suitable dating methods were lacking. Studies that determined the onset of plaggic agriculture using radiocarbon dating and pollen analysis do not give consistent ages (Giani et al. 2014). Furthermore, these ages are not reliable because soil organic carbon is mobile and has probably not been produced in situ and the pollen in the soil profile may originate from other locations as well (Van Mourik et al. 2011). Luminescence dating does not suffer from these problems. Single-grain luminescence analysis is an ideal method for determining both the accumulation and reworking rates, since it determines the ages of plaggic anthrosols much more reliably than radiocarbon dating and palynological analysis (Giani et al. 2014) and it enables analysis of the age distribution within a sample. However, the relatively new feldspar single-grain method has not yet been applied to a plaggic anthrosol nor has it been tested in this particular setting. This study aims to establish a dating method that can provide a reliable age for the first appearance of plaggic agriculture and its development over space and time. Furthermore, it aims to determine the reworking rate and accumulation rate of a plaggic anthrosol in the eastern part of the Netherlands. The single-grain feldspar ages will be compared to independent age estimates for samples from the same location. The research questions that will be answered are:

1. When did plaggic agriculture start to develop at the location of the investigated plaggic anthrosol according to the feldspar single-grain dating method?
2. What are the reworking rates in the plaggic soil and what is the difference between natural and anthropogenic soil reworking?
3. What are the historical accumulation rates in the plaggic soil?
4. How does the single-grain feldspar dating method perform compared to independent estimates including quartz OSL and field observations?

Background

Luminescence dating

Luminescence dating is based on the principle that a latent luminescence signal builds up in a mineral grain (quartz or feldspar) due to the ionising radiation it receives from its surroundings. When the grain is exposed to daylight or heated to a few hundred degrees Celsius the signal is emitted. This signal can be measured, and the luminescence age can be derived from it. Once the exposure to daylight or heating stops, the signal will start to accumulate again. This principle allows calculation of the time that has passed since the grain was deposited, covered by other deposits or brought to the soil surface by reworking processes (Stockmann et al. 2013). In this study the accumulation and emission of the luminescence signal occurs in the context of soil reworking.

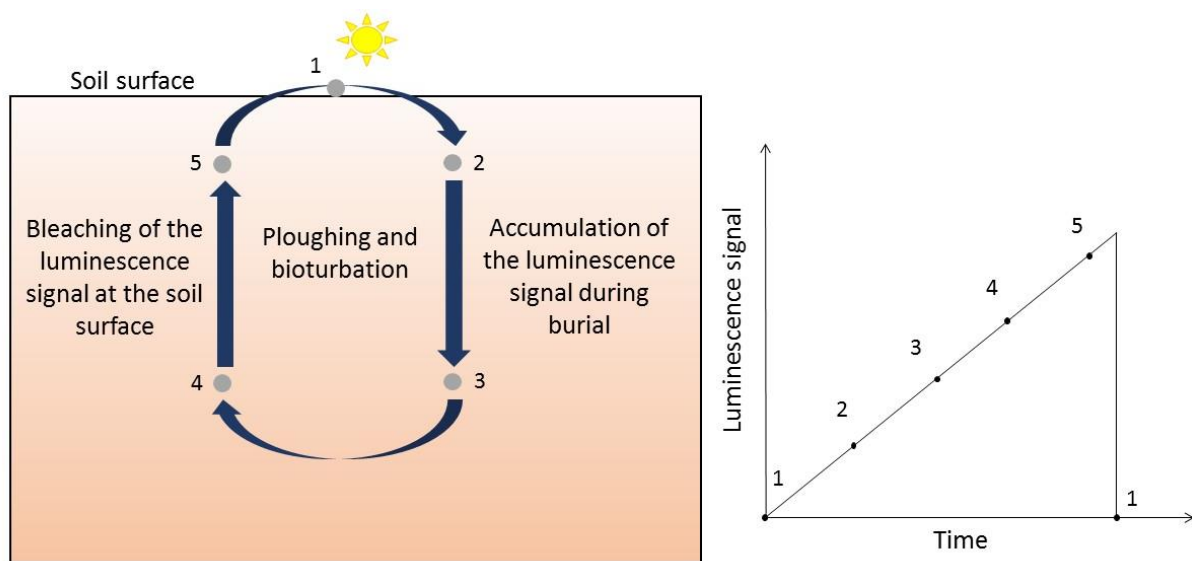


Figure 3 Exposure and burial cycle of a grain as a result of soil reworking. The graph on the right illustrates the build-up of the luminescence signal in the grain during the reworking cycle.

Figure 3 shows the exposure and burial cycle of grains in a soil reworking setting. The exposure and burial cycle is driven by ploughing and bioturbation, or by merely bioturbation when ploughing is absent. The cycle starts when a grain is exposed to daylight (1). During burial, the luminescence signal in a grain builds up due to the ionising radiation it receives from its surroundings (2 to 5). The signal does not necessarily build up linearly with time. This rate depends on the rate at which the grain receives ionising radiation from its environment, which might vary in space and time. When the grain is exposed to daylight again the luminescence signal is emitted or bleached (1) and the cycle starts again. The strength of the accumulated signal per mass of mineral ($1 \text{ J kg}^{-1} = 1 \text{ Gy}$ (Gray)) is the burial dose, which is estimated by the measured palaeodose. Dividing this number by the dose rate, which is the average amount of energy that a mineral receives from its surroundings per year (Gy a^{-1}), gives the luminescence age of the mineral in years:

$$\text{Luminescence age (a)} = \frac{\text{Palaeodose (Gy)}}{\text{Dose rate (Gy a}^{-1}\text{)}}$$

Due to the low energy state of this process, fading only occurs when proximal recombination is possible. A pIRIR stimulation moves extra electrons from the trap into the conduction band tail states. These electrons recombine with the more distant traps and the signal that is emitted in this process is much less affected by fading (Thomsen et al. 2008).

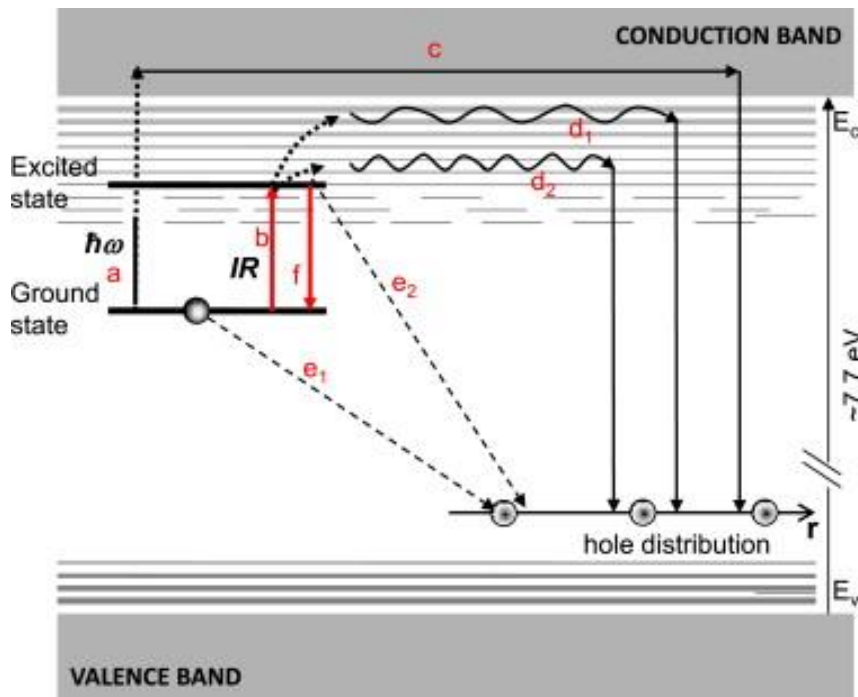


Figure 5 The feldspar infrared stimulated luminescence model by Jain and Ankjærsgaard (2011). Figure from Jain et al. (2015).

Electron traps and recombination centres are the result of lattice defects in the mineral structure that affect the charge. The distance between the trap level and the conduction band is the trap depth. This depth determines how much energy is needed to lift the electron from the trap into the conduction band or the band tail states. The larger this energy, the more likely an electron is to remain captured over larger time scales in a natural setting without fading. Stimulation energy will lift an electron into the conduction band and from there it will recombine with the valence band and release the stored energy in the form of light. The intensity of this light is proportional to the palaeodose, which estimates the true burial dose. The term equivalent dose (D_e), or shortly dose is used more generally for radiation doses derived from a luminescence signal. The radiation dose cannot build up endlessly. The longer a mineral grain is exposed to ionising radiation *and* protected from daylight or heat, the more electrons are trapped and the stronger the latent luminescence signal becomes. Saturation is reached when all recombination traps are filled. The saturated luminescence signal depends on the type of mineral and it represents the maximum age that can be determined for that mineral.

Dose rate

Types of ionising radiation that contribute to the dose rate are alpha, beta and gamma radiation and cosmic rays. Alpha radiation consists of He nuclei, beta radiation of electrons and gamma radiation of photons. Compared to beta and gamma radiation, alpha radiation has a much shorter penetration depth. It only penetrates the outer part of sand-sized grains. Smaller grains like silt and clay are fully penetrated by all three radiation types. Another property of alpha radiation is that it results in a weaker luminescence signal with respect to the amount of absorbed radiation than beta and gamma radiation.

The environmental dose rate that is needed for luminescence age calculation is the sum of internal radiation, external radiation and cosmic radiation. Internal radiation is produced within the mineral grain itself. The most important source of internal radiation is ^{40}K , which is present in alkali feldspars but not in quartz. For that reason, internal radiation is often neglected for quartz but not for feldspar. External radiation is the radiation that a mineral grain receives from the surroundings. It mainly originates from the $^{238}\text{U}/^{235}\text{U}$ and ^{232}Th decay chains and from ^{40}K in feldspars, micas and clay minerals. Other radioactive elements in the surroundings generally contribute very little to the external radiation, so they are neglected. An important factor to consider in external dose rate calculations is the moisture content of the sediment, because moisture attenuates the radiation coming from surrounding grains much more than air. Cosmic radiation consists of particles from outside our solar system that penetrate the Earth surface. The Earth magnetic field causes the intensity of cosmic radiation to be larger near the poles and the amount of cosmic radiation absorbed by a mineral grain decreases with increasing water and sediment overburden.

Measuring soil mixing using single-grain luminescence

Conventional multiple grain luminescence dating is based on the assumption that post-depositional mixing is absent or negligible. Mixing of the profile used to be an obstacle for age determination and process interpretation. When single-grain analysis was developed, it was a tool to 'correct' for bioturbation processes. Lately it has been used to study the mixing processes themselves (e.g. Kristensen et al. 2015, Gliganic et al. 2016). Single-grain luminescence is especially relevant for soils, because soils are subjected to mixing, whereas conventional multiple grain luminescence is used for unmixed layered sediments. When luminescence dating is performed on single grains, the dose distribution of the grains in one sample reveals the ages of grains present at one location. Soil mixing rates can be estimated from the equivalent dose distribution in a certain sample (Figure 6) (Bateman et al. 2003).

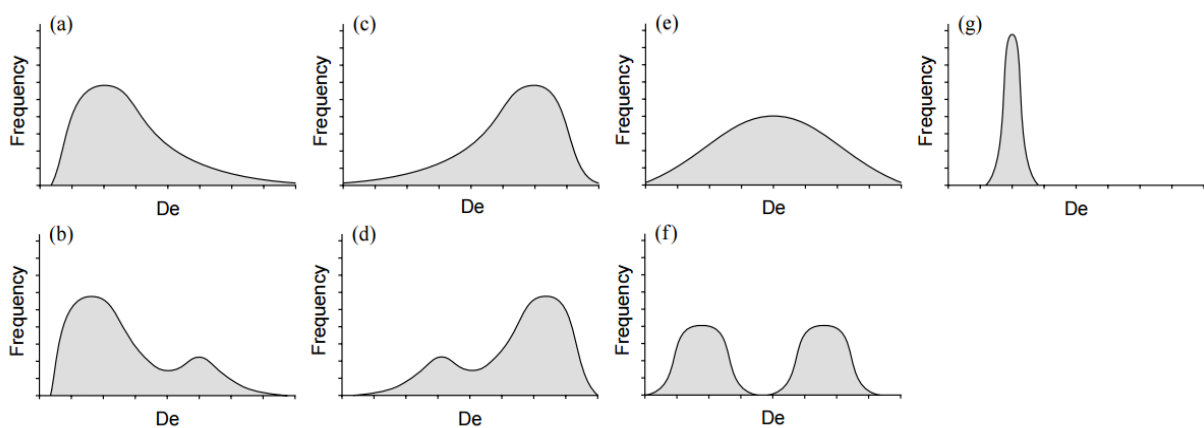


Figure 6 Potential dose distributions in a sample. Figure from Bateman et al. (2003).

The more mixing has occurred, the more younger and older grains have been introduced in the original grain composition, the wider the dose distribution becomes (compare Figure 6 e and g). This happens for example because of mixing by soil fauna such as earthworms (Wilkinson et al. 2009). A skewed distribution with a left tail (Figure 6 c and d) occurs when an old sample received younger grains, for example by movement of younger grains downward in the soil profile through former root channels (Hülle et al. 2009). A tail on the right (Figure 6 a and b) means that a younger sample has received older

grains. Skewed distributions are normally the result of minor mixing processes whereas a wide normal distribution is the result of intensive mixing (Bateman et al. 2003). A multi-modal distribution (Figure 6 b, d and f) reflects separated phases of mixing. In that case, only one peak will refer to the age of deposition, the other peaks are related to the mixing phases and represent the ages of the material that is mixed into the sample (Bateman et al. 2003).

Single-grain quartz dating

Quartz grains do not yet show a luminescence signal when they are extracted from weathered plutonic and volcanic bedrock. Only when they are bleached upon reaching the surface and exposure to daylight, they become sensitive to ionising radiation. During following exposure and burial cycles, this sensitivity to radiation increases. This maturing or sensitisation phenomenon has been observed by Pietsch et al. (2008) for fluvial settings, by Sawakuchi et al. (2012) for coastal settings and recently by Reimann et al. (2017) in the context of soil reworking. Single-grain quartz luminescence dating has already proved itself useful for quantification of grain mixing through the soil column. Heimsath et al. (2002) determined the movement of individual quartz grains caused by soil creep on an Australian hillslope. They derived the vertical mixing rate from the time that has passed since the grains last visited the soil surface. They found that the mean age increases with depth, but that still a substantial amount of finite-age grains is present near the soil base. They also found that the mean finite age is much smaller than the residence time of grains in the soil. From this they concluded that a substantial part of the grains must visit the soil surface several times. Stockmann et al. (2013) used single-grain quartz OSL to derive soil mixing rates in a forest in Australia using the following formula:

$$\text{Soil mixing rate (mm/year)} = \frac{\text{Depth of burial (mm)}}{\text{OSL age (year)}}$$

In line with the results by Heimsath et al. (2002), the proportion of finite-age grains and zero-age grains decreased with soil depth and median ages increased with soil depth. They concluded that the probability of grains experiencing repeated cycles of exposure decreases with depth and that pedoturbation was not intensive enough to cause homogenised distributions. Another application of the single-grain quartz method is found in Kristensen et al. (2015). A termite mound was sampled at several depths below ground and inside the mound. Vertical transport processes were observed and quantified. The main transportation process was found to be a vertical 'conveyor belt' in which the termites transport grains upward into the mound. At the same time the mound slowly erodes so that grains from the top of the mound are bleached and deposited near the bottom. This enables determination of the upward transport rate. The luminescence signal from single grains does not only contain information on soil movement and turnover rates. It can also be used for identification of periods of more intensive mixing. Gliganic et al. (2015) used the single-grain quartz method to reconstruct phases of enhanced post-depositional mixing in an alluvial fan in Australia. These phases of enhanced pedoturbation are hypothesised to represent warmer, more humid climatic conditions. Alluvial fans are a well layered type of deposits. Single-grain dose distributions were analysed with the finite mixture model to find the ages of grains that moved into layers of other ages. The component that contained most grains was assumed to be representative for the time of deposition. Younger minor components represent grains from higher up in the soil profile that have been transported downward by mixing processes. Older components might be the result of both mixing processes and incomplete bleaching. Incomplete bleaching is a common phenomenon in fluvial deposits, since they have been shielded from daylight during deposition. Aeolian deposition, on the other hand, will result

in complete bleaching. Phases of aeolian dune aggradation and subsequent modern mixing processes were identified and modelled by Gliganic et al. (2016). Their soil profile consisted of layered aeolian deposits that were mixed by subsequent bioturbation. This mixing was so strong that the depositional ages could not be determined, because the finite mixture model did not give reliable ages. A combination of the minimum age model and a mixing zone model resulted in the identification of three mixing phases.

Single-grain feldspar dating

Until now single-grain luminescence dating has been mainly applied to quartz grains (e. g. Heimsath et al. 2002, Stockmann et al. 2013, Gliganic et al. 2015, Kristensen et al. 2015, Gliganic et al. 2016). These studies are often performed in areas where quartz grains show exceptionally good luminescence properties (e. g. Heimsath et al. 2002, Stockmann et al. 2013). The luminescence signal of quartz grains from Australia, for example, is a few orders of magnitude brighter than that of European quartz grains (Pietsch et al. 2008), which is considerably more convenient for measurements. However, in most cases the single-grain quartz OSL method is time consuming and labour intensive as only 1 to 5 % of the quartz grains have a luminescence signal that is bright enough for accurate measurement (e. g. Duller 2008, Demuro et al. 2013). An additional disadvantage of the single-grain quartz method are the sensitivity changes resulting from repeated exposure and burial cycles (Murray and Roberts 1998).

A more widely applicable single-grain method was recently proposed by Reimann et al. (2017). They used individual sand-sized feldspar grains as soil reworking tracers to reconstruct soil reworking rates for a soil profile in Spain. The advantages of this method over the single-grain quartz method are that many feldspar grains emit a suitable luminescence signal, also if they have never been exposed to daylight (Duller 2006, Reimann et al. 2012), that the luminescence signal of feldspar grains does not depend on the number of exposure and burial cycles that it has experienced (Lukas et al. 2007), and that a large fraction of the environmental dose rate originates from ^{40}K inside the feldspar grain, which minimises the inaccuracies arising from the assumption that the external radiation field was constant over the entire burial time (e. g. Reimann et al. 2011). A disadvantage is that feldspar IRSL signals are subject to anomalous fading (Spooner 1994), which means that trapped electrons in the ground state slowly recombine to less energetic levels near the valence band through tunnelling, leading to measurement of a weaker luminescence signal and thus to age underestimation. Another disadvantage of using feldspar grains to determine soil reworking rates is that feldspar grains need a longer daylight exposure time than quartz grains to bleach completely because the bleaching rate is slower (Godfrey-Smith et al. 1988). This effect is stronger for pIRIR signals than for the IRSL signals (Godfrey-Smith et al. 1988, Murray et al. 2012). This increases the probability of incomplete bleaching and thus of age overestimation. The method by Reimann et al. (2017) minimises both disadvantages. Low-temperature (< 200 °C) IRSL and pIRIR feldspar signals are used, because they are better bleachable than high-temperature signals (Kars et al. 2014). This low temperature pIRIR signal is also less sensitive to anomalous fading according to Reimann et al. (2011).

Secondly, they propose a novel way to calculate the soil reworking rate. Until now, calculations of the soil reworking rate as used by e. g. Stockmann et al. (2013) did not consider the proportion of mineral grains that never reached the surface. They determined the reworking rate from the grains that showed a suitable luminescence signal only. Reimann et al. (2017) argue that this is only an apparent reworking rate (SR_{app}), as it does not take into account the depth dependency of soil reworking. They introduced the non-saturation factor (NSF), the proportion of non-saturated grains to the total number

of grains that were used in the analysis, to correct for the grains not participating in reworking (the so-called 'out of competition' grains with a reworking rate of 0 mm y^{-1}). The apparent reworking rate multiplied by the NSF gives the effective soil reworking rate (SR_{eff}), which is dependent on depth. The more grains are out of competition, the smaller the effective reworking rate is compared to the apparent reworking rate. The results of the feldspar single-grain method were compared to the results of the more conventional quartz single-grain method. The feldspar SR_{eff} is dependent on depth, whereas the quartz SR_{eff} is similar for each of the upper three samples but much lower for the lowest sample. Because quartz grains recently derived from weathered bedrock mature and sensitise during the repeated cycles of exposure and burial, the quartz grains that do not show a suitable luminescence signal are the weathered bedrock grains that have not been reworked. This gives a bias in the SR_{eff} estimated from quartz. The feldspar luminescence signal does not change over time, so the feldspar- SR_{eff} are a better estimate of the reworking rate than the quartz- SR_{eff} .

Analysis of single-grain distributions

Apart from the type of mixing process that can be derived from the shape of a single-grain distribution (Figure 6), there is often a need for quantitative information. In most cases this includes the palaeodose of one or more peaks in a sample distribution. Statistical age models have been developed to identify these peaks. The most commonly used ones are discussed below. The choice for an age model must always be made considering prior knowledge of a sample, such as the sedimentary context and the bleaching state that is expected based on for example the depositional environment. The different single-grain dose distributions in Figure 6 require different methods of analysis, depending on the type of distribution and the type of age (minimum age, maximum age, etc.) that needs to be derived. Age models are usually applied to the log-transformed equivalent dose measurements, because their errors are symmetrically distributed. This log-transformation requires that the equivalent dose dataset exclusively consists of positive estimates. However, for samples containing near-zero aged grains some measurements will give negative equivalent dose values. The age models can also be applied to the unlogged equivalent dose measurements, but for samples older than approximately 350 years this may lead to underestimation of the burial age (Arnold et al. 2009). Age models can be bootstrapped, which means that they measure the statistical properties (e.g. age and spread in the age distribution) of a sample by taking subsets from the sample and determining the average statistical properties for these subsets. This allows for inferences about statistical properties of the population from measurements on the sample, because the relation between a sample subset and a sample is assumed to be the same as the relation between a population and a sample (Efron and Tibshirani 1993, Cunningham and Wallinga 2012).

In addition to the age, the spread in a single-grain D_e distribution is often assessed. This spread has several sources. Experimental errors are the errors of the combined measurements (counting statistics), the Monte Carlo fitting error and the error of the measurement equipment. The spread in the equivalent dose distribution that is not explained by these experimental errors is called the overdispersion. The overdispersion can partially be explained by variations in natural circumstances like mixing and poor bleaching, but even for a sample that is known not to be mixed after deposition and for which deposition has occurred instantaneously and after complete bleaching, still a certain amount of overdispersion is present. This is called the minimum overdispersion σ_b . One of the sources of this minimum overdispersion is for example a spatially and temporally heterogeneous dose rate in the radiation field (Olley et al. 1997).

Weighted mean age models

When the single-grain D_e distribution is normally distributed with only a few outliers, the age of interest is often the mean age. In the calculation of the mean D_e the errors of the individual measurements are used as a weighting factor. An error-weighted mean age reduces the influence of grains having a large dose measurement error and gives more weight to grains of which the equivalent dose was determined more precisely. There are two types of weighted mean age models. The common age model determines the weighted mean as a single value without standard error whereas the central age model (CAM) determines the weighted mean as a normal distribution of ages (Galbraith et al. 1999). The latter is more often used for luminescence dating purposes.

Minimum age model and maximum age model

The minimum age model of Galbraith et al. (1999) estimates the equivalent dose corresponding to the youngest, leading-edge population in a sample distribution. This model is often applied to fluvial samples, because fluvially deposited grains are often not completely bleached before burial (e. g. Arnold et al. 2007, Pietsch et al. 2008). As described in (Galbraith and Roberts 2012), the minimum age model fits a truncated normal distribution to the logged equivalent dose values. The lower truncation point is assumed to correspond to the average dose of the leading-edge population. In the four-parameter minimum age model (MAM-4), the lower truncation point γ is smaller than the mean of the normal distribution μ . The other two parameters of this model are the standard deviation σ and the proportion of fully bleached grains p . When the lower truncation point coincides with the mean of the normal distribution ($\gamma = \mu$), the model contains only three parameters (MAM-3). This three-parameter model is more commonly used than the four-parameter model.

The maximum age model is essentially an inversion of the minimum age model by Galbraith et al. (1999). Instead of determining the dose of the youngest subpopulation, it determines the dose of the oldest subpopulation. All parameters are the same, except that γ is now defined as the upper truncation point. This model can be used when the age of interest corresponds to the maximum peak in the single-grain dose distribution. This might be a situation in which the age of older grains mixed into a sample needs to be determined or when the burial age must be derived from a sample that has been mixed and bleached by bioturbation.

Finite mixture model

When prior knowledge on a sample setting indicates that a sample contains more than one dose population, the finite mixture model (FMM) can be used to identify the separate populations. This model fits several normal distributions to the sample distribution. Each fitted distribution accounts for one population. If the number of subpopulations is known, the finite mixture model can be applied directly specifying the number of components. However, sometimes the number of subpopulations is not known exactly. In that case, the number of components needs to be estimated first. The FMM can not only be used to identify the average equivalent dose and proportion of each subpopulation, it can also estimate the number of subpopulations. The finite mixture model can be run multiple times for different numbers of components and the outputs of each of these runs can be compared based on their BIC value (Bayes Information Criterion, (Schwarz 1978)). The lower this number, the better the combined fit of the components. The number of components that results in the lowest BIC-value is then the best estimate for the number of subpopulations in a sample population. The minimum overdispersion of the normal distributions that are fitted to the sample distribution must be specified in advance. It is important to know the overdispersion accurately, especially when estimating the

number of components, because they are closely coupled. The finite mixture model assumes all components to have the same overdispersion. In a lot of cases this assumption may not be true, for example when the components in a sample do not have the same sedimentary history, or when one component is the result of post-depositional mixing whereas the other component consists of unmixed grains. Because the finite mixture model identifies all peaks in a sample distribution, it can be used to estimate the maximum and minimum components as well. An advantage of the FMM over the minimum and maximum age model is that it also calculates the proportion of grains in each component. A disadvantage of calculating these ages with the FMM is that the estimates for the component of interest are dependent of the estimates of the remaining components, because the proportions of all components must add up to one.

Sampling location and site description

Samples were taken in a plaggic anthrosol in the east of the Netherlands south of Denekamp. The coordinates of this location in the Dutch *RD new* coordinate system are $x=266141$, $y=486424$. According to the map by Niemeier and Taschenmacher (1939) in Figure 2, plaggic soils have been found in this area. The digital elevation model of this location in Figure 7 clearly shows that the surface elevation of some fields is higher than that of their surroundings. Field observations confirmed this. These higher fields are the plaggic soils. West of the sampling location are the small river Dinkel and the Dinkel valley. The area around the sampling location is part of the European sand belt that stretches from northwestern Europe into Poland and the Baltic region (Zeeberg 1998). The parent material of this sand belt is Pleistocene cover sand, so the soils that are formed are relatively nutrient poor. The (palaeo)soils that lie in the European sand belt are mostly podzols. A study by Smeenge (in preparation) has showed that at the sampled location plaggic agriculture has been practised at least since 1132 ± 93 AD. This age estimate is derived from quartz OSL measurements by Smeenge (in preparation).

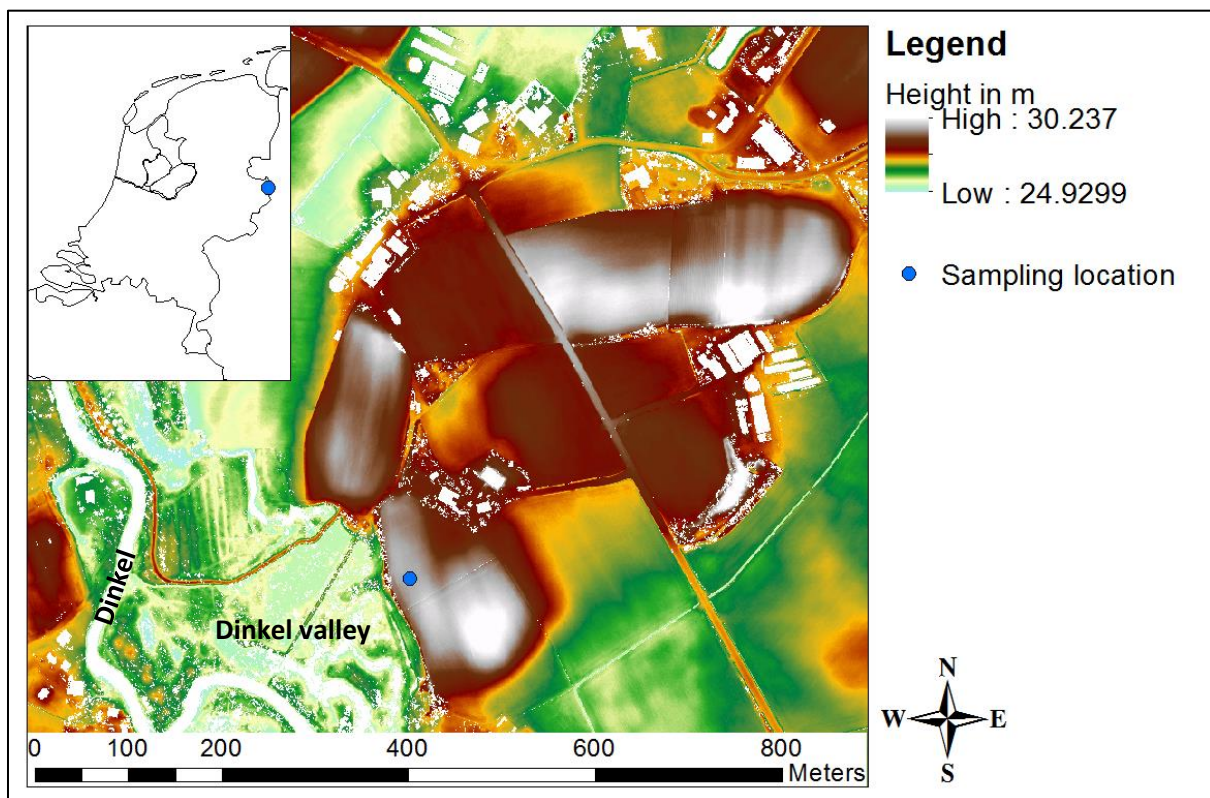


Figure 7 Digital elevation model of the study area. The DEM is the *interpolated AHN2 0.5 meter ground level raster* of the Dutch Actueel Hoogtebestand Nederland (AHN 2012). The inset map was downloaded from thematicmapping.org on 14 July 2017 (Sandvik 2009).

Experimental methods and details

Soil description and classification

A soil pit was dug and the soil horizons and their Munsell colour were determined (Table 1). At all depths, the texture was classified as weakly loamy sand with a median grain size of 210 μm . The plaggic layer consists of two Aap horizons that differ from each other in colour (Figure 8). The Aap1 horizon is darker than the Aap2 horizon, which could indicate that different plaggen types were used. The light colour of the Aap2 horizon might be derived from forest or heather plaggen while the darker colour might be derived from peat plaggen, possibly taken from the lower lying Dinkel valley. A transition horizon separates these plaggic layers. This transition horizon has an intermediate colour and in addition brown and lighter coloured spots were observed. As a result of ploughing this transition horizon is rather thick with indistinct upper and lower boundaries. Below the plaggic horizons a non-plaggic light coloured ploughing layer was identified. The light colour of this layer is partly caused by the presence of grey coloured grains that strongly resemble the grey grains normally found in the eluviation horizon of a podzol. The unploughed part of the soil consists of a brown weathering horizon (Bw) and cover sand parent material in which gleyic phenomena were observed (Cg). The thick plaggic layer and the human influence on this soil are the main reasons that this soil was classified as a plaggic anthrosol.

Table 1 Soil horizon descriptions at the sampled location.

Depth (cm)	Horizon	Munsell colour	Remarks
0-30	Aap1	10YR 2/2	Small pieces of brick
30-50	Aap1/Aap2	10YR 3/2	Small pieces of brick, brown and lighter coloured spots
50-105	Aap2	10YR 3/3	Black spots up to \pm 80 cm depth
105-120	Ap	10YR 4/2	Podzol-grey coloured grains present
120-130	Bw	10YR 4/3.5	
130-170	Cg	2.5Y 5/4	Some fossil gley mottles of several cm in size present at 150-160 cm depth.

The soil that was present at this location before the start of plaggic agriculture consists of Ap, Bw and Cg horizons. It is clear that the original soil was not a classical poor podzol, because no eluviation (E) and Bh horizons were found. The Bw horizon indicates that the original soil was a brown forest soil, but the presence of podzol-grey coloured grains seems contradictory. The richness in organic matter of the Ap horizon and the gleyic mottles in the Cg horizon do not support poor podzols. There are several possible explanations for the presence of podzol grains in the Ap horizon. It could be that a thin podzol was already present at this location before it started to be used for agriculture. This podzol must have been so thin that it was completely mixed by ploughing. However, it is not very likely that a podzol in cover sand of Pleistocene age was thin, given the long development time. Maybe the grey grains indicate that the original brown forest soil was already degrading towards a poor podzol. The grey grains are not necessarily formed in situ. They may also have been included in the earliest applied plaggen sods cut from a podzol topsoil and then mixed through the ploughing horizon. Another possibility is that the grey grains have originated from a nearby podzol and were deposited by the wind during a period of drift sand activity. If the grey grains originate from elsewhere, whether by plaggen application or by aeolian deposition, no palaeo-podzol has been present at this location. If the grey grains have been formed by soil degradation, no fully developed palaeo-podzol has been present either. Therefore, the original soil below the plaggic layers is assumed to be a brown forest soil.

Sampling

Thirteen luminescence samples were taken at the depths indicated in Figure 8. Sample NCL-1117128, NCL-1117130 and NCL-1117134 served as extra samples and they were not dated. For each sample, a pvc tube of 20 cm in length and 4.5 cm in diameter was hammered horizontally into one of the pit walls. The tubes were removed taking care not to disturb the sample. They were closed with lids and tape on both ends. Extra soil material from the same depths as the tubes was collected in plastic sample bags for dose rate determination.

Figure 8 Soil profile at the sampling location. The sample numbers on the left correspond to the sampling tubes in the picture. Samples NCL-1117128, NCL-1117130 and NCL-1117134 were not dated.

NCL-1117134 (22 cm)
NCL-1117133 (31 cm)
NCL-1117132 (41 cm)
NCL-1117131 (50 cm)
NCL-1117130 (60 cm)
NCL-1117129 (70 cm)
NCL-1117128 (81 cm)
NCL-1117127 (96 cm)
NCL-1117126 (101 cm)
NCL-1117125 (112 cm)
NCL-1117124 (123 cm)
NCL-1117123 (142 cm)
NCL-1117122 (165 cm)



Measurements

All samples were unpacked in a dim orange light environment. The outer 3 cm of soil material in each tube was removed to be used for dose rate estimation. This material may have been exposed to daylight, so it was not used for estimation of the equivalent dose. Only the material from the inner part of the tube was used for estimation of the equivalent dose.

Dose rate

Dose rate material was dried in aluminium containers at 105 °C to remove any moisture. The difference in weight before and after drying reflects the soil moisture content. Subsequently, the dried samples were ashed at 500 °C to remove all organic material. The difference in weight before and after ashing reflects the organic matter content. Organic matter content and water content are both needed for estimation of the external dose rate attenuation. The samples were sieved and grinded to reduce the particle size to <math><300 \mu\text{m}</math>. Molten wax was mixed with dose rate material to make a puck of 2 cm thickness. Using gamma spectrometry, this puck was analysed for the activity of isotopes in the Uranium and Thorium decay chains (contributing to the external dose rate), the ^{40}K activity (contributing to both the external and internal dose rate) and the ^{87}Rb activity (contributing to the internal dose rate). The ^{40}K and ^{87}Rb activities inside feldspar grains were assumed to be $10 \pm 2 \%$ and $400 \pm 100 \text{ ppm}$ respectively as proposed by Smedley et al. (2012). The contribution of cosmic radiation to the dose rate was determined as described by Prescott and Hutton (1994). The total dose rate was derived from the internal and external components and the cosmic radiation component.

Equivalent dose

The inner material from the tubes was used for measurement of the equivalent dose. Approximately 100 grams of soil material from each sample were weighed in a beaker, mixed with water and sieved to separate the size fractions <212 μm , 212-250 μm and >250 μm . After sieving, the size fraction 212-250 μm was cleaned by magnetic separation. This removes all magnetic particles, so that the remaining grains are mainly quartz and feldspar and some other non-magnetic minerals. Further cleaning consisted of adding an excess of 10% HCl to remove calcium carbonates and an excess of 10% H₂O₂ to remove organic material. For luminescence measurements, organic material must not be removed by ashing, because the elevated temperature will affect the luminescence signal of the grains. K-feldspar grains having a density of 2.57 g/cm³ were separated from the quartz grains (2.64 g/cm³) and the heavier Ca and Na feldspars by density separation using LST heavy liquid of 2.58 g/cm³.

The luminescence signal of the feldspar grains was measured using an automated Risø TL/OSL reader (DA 15) fitted with a red and green laser single-grain attachment. The grains were stimulated for 1.68 s with a 150 mW 830 nm IR laser. All feldspar grains were detected through a LOT/Oriel D410/30 interference filter to select the K-rich feldspar emission around 410 nm. For dose-response measurements a ⁹⁰Sr/⁹⁰Y beta source irradiated the samples at a dose rate of 0.1145 Gy/s. For single-grain measurements aluminium single-grain discs with a 10x10 grid of 300 μm grain holes were used to ensure that exactly one feldspar grain of size 212-250 μm fits in one hole.

First the rough equivalent dose of the samples was estimated with multiple grain D_e measurements. The equivalent dose estimates were used to optimise the single-grain equivalent dose measurement protocol. To test the performance of the measurement protocol, a single-grain dose recovery test was performed on samples NCL-1117123 and NCL-1117129. Two components of the feldspar luminescence signal were measured: first the infrared stimulated luminescence signal at 50°C (IRSL₅₀) and then the post-infrared signal at 175°C (pIRIR₁₇₅). The samples were bleached in a solar simulator for 45 hours, receiving simulated daylight five times as strong as natural daylight. The remaining signal was measured as the laboratory residual dose. Subsequently dose recovery measurements were performed, and the laboratory residual dose was subtracted from the recovered doses. This yielded the dose recovery ratios in Table 2.

Table 2 Dose recovery ratios for the IRSL and pIRIR signal of sample NCL-1117123 and NCL-1117129. The number of grains used for residual dose measurement (n_{res}) and dose recovery measurement (n_{DR}) are indicated between brackets for each dose recovery ratio.

Sample	pIRIR	IRSL
NCL-1117123	0.97 ± 0.04 (n _{res} = 15, n _{DR} = 81)	1.00 ± 0.03 (n _{res} = 54, n _{DR} = 106)
NCL-1117129	0.99 ± 0.05 (n _{res} = 23, n _{DR} = 24)	0.92 ± 0.04 (n _{res} = 6, n _{DR} = 22)

Three of the four ratios are consistent with 1 within 1 σ . The dose recovery ratio of the IRSL signal for sample NCL-1117129 is a bit low. This value is based on a small number of grains, which might explain why this value differs from the other values. However, the value still is consistent with 1 within 2 σ . The equivalent dose measurements of the natural signal and the laboratory doses were performed using a low pre-heat of 200°C for 120 s, an infrared stimulation at 50°C for 1.68 s, a pIRIR stimulation at 175°C for 1.68 s and a cut-heat of 210 °C for 40.0s. Table 3 shows the steps of this protocol.

Table 3 Steps of the equivalent dose measurement protocol.

Step	Treatment	Measurement
1	Natural or regenerative dose	
2	Preheat at 200°C for 120 s	
3	Infrared stimulation at 50°C for 1.68 s (single grain)	L _x IRSL ₅₀
4	Infrared stimulation at 175°C for 1.68 s (single grain)	L _x pIRIR ₁₇₅
5	Test dose	
6	Preheat at 200°C for 120 s	
7	Infrared stimulation at 50°C for 1.68 s (single grain)	T _x IRSL ₅₀
8	Infrared stimulation at 175°C for 1.68 s (single grain)	T _x pIRIR ₁₇₅
9	Cut-heat at 210°C for 40.0 s	

All equivalent dose measurements were analysed using the Risø Luminescence Analyst software version 4.31.9 (Duller 2015). Each dose-response curve was fitted exponentially through the regenerative dose points and forced through the origin. Errors were not incorporated in curve fitting. Instead the curves were fitted using 1000 Monte Carlo repeats and a measurement error of 2.5 %. The integration limits for the signal were set from channel 5 to 7 and for the background signal from channel 40 to 50. With a channel size of 0.03 s, this leads to measurement of the signal between 0.15 and 0.21 s and measurement of the background signal between 1.20 and 1.50 s after the start of stimulation. None of the acceptance criteria within the software was applied. Acceptance criteria were applied manually and included the following (after Reimann et al. (2017)):

1. A test dose error smaller than 20% of the test dose signal
2. A natural test dose signal greater than the background test dose signal
3. Recycling ratio within 2σ from unity
4. Monotonically growing dose response curves

The first two criteria assess whether the grain emits a sufficiently bright luminescence signal or not. The third criterion excludes all grains that are subject to sensitivity changes during the repeated measurement cycles. The fourth criterion was assessed visually and by checking the ‘average error in fit’ as reported by the Risø Luminescence Analyst software. It excludes all grains for which no consistent exponentially growing dose response curve could be fitted.

Minimum age calculation

To enable comparison between the samples, an overall age needs to be determined for each sample. The age of interest in the context of soil reworking is the moment of latest reworking, because this gives the moment of latest bleaching of the mineral grains in the soil, which is the moment that the grains were buried below the ploughing layer. The minimum age or leading-edge D_e represents this moment. For the samples in this study, there are several ways to find this age. The most common way would be to apply the minimum age model to the equivalent dose datasets. This results in a minimum D_e which can be converted to a minimum age using the dose rate. Because the minimum dose corresponds in most samples to the main peak in the distribution, another method that works well in this context is to calculate the iterated weighted mean D_e . During iteration, outliers are removed until the weighted mean reaches a stable value. The leading-edge D_e has been calculated using the minimum age model and the iterated weighted mean for both the IRSL and pIRIR signal (Figure 9) according to the detailed methods in the next sections. The most appropriate combination of signal and age model was selected based on the results.

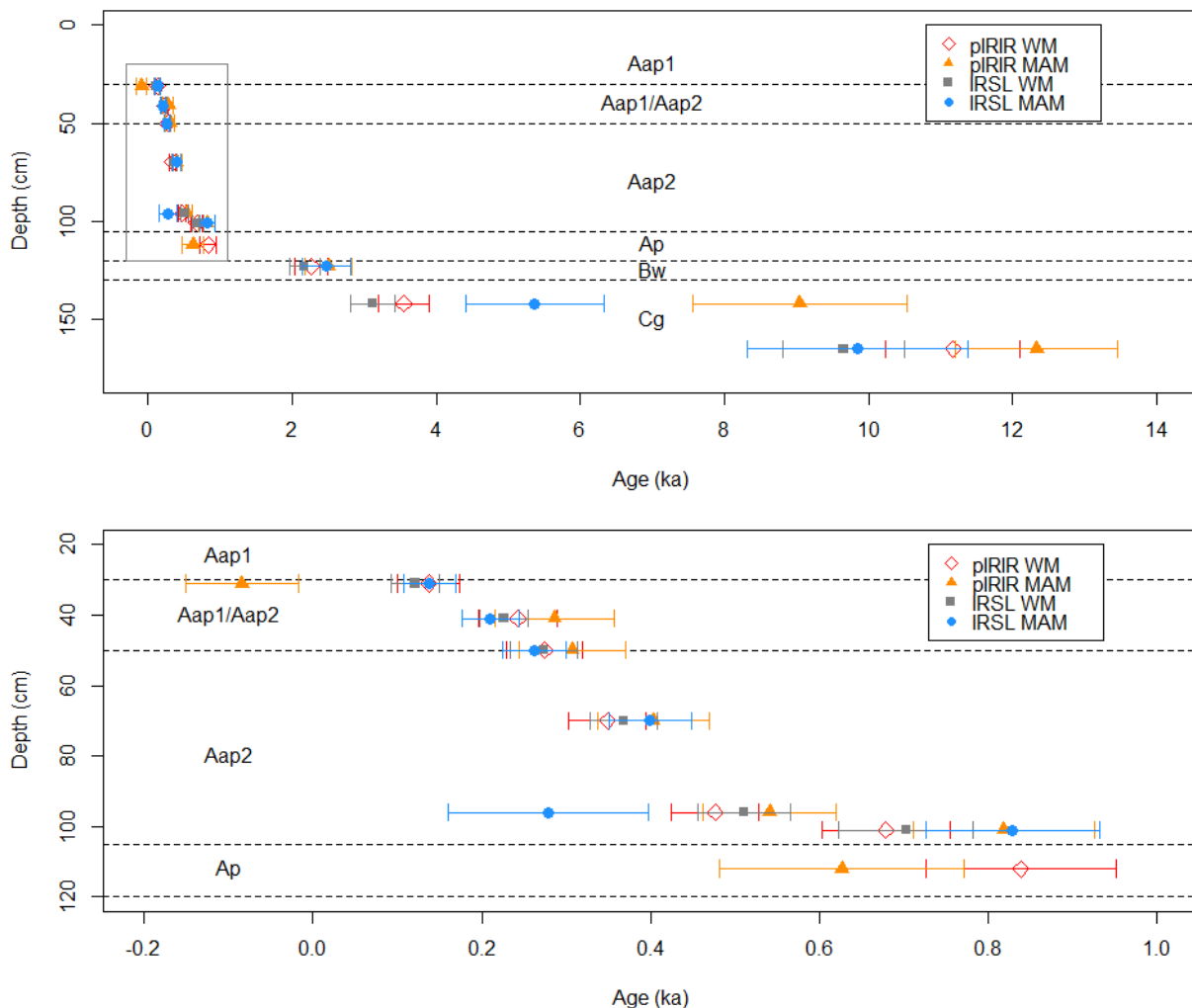


Figure 9 Age-depth profiles and soil horizons for the iterated weighted mean (WM) and the minimum age model (MAM) for both signals. The upper graph shows the whole profile and the lower graph shows the section indicated in the upper graph in more detail.

Minimum age model

The equivalent dose datasets were loaded in Matlab (version R2017b) and the overdispersion for both the IRSL and pIRIR signal of each sample was calculated using the bootstrapped central age model (Cunningham and Wallinga 2012) of Galbraith et al. (1999). These overdispersion values per sample can be found in Appendix Table 6. Subsequently the minimum overdispersion values per signal (σ_b) were found by applying the bootstrapped three-parameter minimum age model (Galbraith et al. 1999, Cunningham and Wallinga 2012) to the sample overdispersion values. The minimum overdispersion was found to be $33 \pm 4 \%$ for the IRSL signal and $43 \pm 2 \%$ for the pIRIR signal. The bootstrapped three-parameter minimum age model (Galbraith et al. 1999, Cunningham and Wallinga 2012) was then applied to the D_e datasets using the minimum overdispersion as input to find the MAM D_e values (Appendix Table 7). For some of the samples, the conventional, logged version of the model could not be applied because of negative D_e values present in the dataset. For these samples the unlogged version of the model was used. The MAM D_e values were converted into a MAM age using the dose rate and then corrected for fading of the feldspar signal using the function *calc_FadingCorr* in the R package *Luminescence* with *tc* (time in seconds between irradiation and the prompt measurement) set to 2592000 s, *tc.g_value* (time in seconds between irradiation and the prompt measurement used for estimating the g-value) set to 172800 s and 100 Monte Carlo repeats. This R function is based on the fading correction proposed by Huntley and Lamothe (2001). Fading rates (g-values) used for the fading correction were determined by applying the R function *analyse_FadingMeasurement* to laboratory fading measurements. The fading rate of the IRSL signal was $4.0 \pm 0.5 \%$ /decade and the fading rate of the pIRIR signal was $1.5 \pm 0.2 \%$ /decade. After fading correction, a poor bleaching correction was applied based on comparison of the feldspar age and corresponding quartz ages, which are independent age estimates measured by Smeenge (in preparation). Since these quartz ages were measured at different depths than the feldspar ages in this study, the quartz ages corresponding to the depths of the feldspar ages were determined by linear interpolation of the age-depth gradient between samples. The poor bleaching correction factors were determined as the error-weighted mean difference between the feldspar age and the quartz age, in which the error of the feldspar age was used as the weighting factor. The correction factors for poor bleaching of the feldspar signal were found to be -0.23 ± 0.03 ka for the pIRIR MAM age and $+0.03 \pm 0.02$ ka for the IRSL MAM age. The positive correction factor implies that the feldspar IRSL signal is better bleached than the quartz signal. This is unlikely to be true since the feldspar signal bleaches more slowly than the quartz signal (Godfrey-Smith et al. 1988, Thomsen et al. 2008), so correction of the IRSL MAM age might be unnecessary. However, the correction was still applied for calculation consistency with the other ages calculated in this study. The pIRIR correction factor was determined based on eight pairs of quartz and feldspar pIRIR ages and the IRSL correction factor was determined based on seven pairs of quartz and feldspar IRSL ages (for the depths of sample NCL-1117124 and upward, no IRSL measurements for sample NCL-1117125). The corresponding quartz ages for the oldest two feldspar samples could not be interpolated because the deepest quartz age by Smeenge (in preparation) was measured at a depth of 130 cm, which is above the deepest two feldspar ages.

Iterated weighted mean age

In order to calculate the iterated weighted mean age for both signals and for each sample, first the error-weighted mean D_e values were calculated. Then all D_e values that were not consistent with the error-weighted mean within 2σ were iteratively removed until the error-weighted mean was stable. This value was converted to an age using the dose rate and a fading correction and a poor bleaching correction were applied in the same manner as described above for the minimum age. The poor bleaching correction factors were -0.19 ± 0.02 ka for the pIRIR iterated weighted mean age and -0.08 ± 0.01 ka for the IRSL iterated weighted mean age.

Selection of signal and age model

The age of the leading-edge population can be calculated using either the MAM-3 or the iterated weighted mean, based on either the IRSL signal or the pIRIR signal. The most suitable signal and age model were selected based on the results for the four combinations of signal and age model. First the most appropriate signal was chosen based on a comparison of bleaching and fading issues and then the most suitable age model was chosen based on the internal stratigraphic consistency of the age-depth profiles and their consistency with age expectations based on literature.

To find out whether fading or poor bleaching is a bigger problem for the samples in this study, the D_e distributions for both signals of sample NCL-1117122 were checked. This is the deepest and oldest sample and also the most undisturbed sample, so the effects of poor bleaching and fading should be best visible here. The most striking feature of this sample is that the IRSL distribution shows a double peak. This might be caused by the characteristics of this sample, but it could also be a statistical artefact. Because the other samples do not show such double peaks (see IRSL radial plots and D_e distributions of the other samples in the Appendix), this observation is not used for interpretation. The IRSL distribution of sample NCL-1117122 is also broader than the pIRIR distribution (Figure 10). This might point at reworking that is picked up by the IRSL signal but not by the pIRIR signal. In that case poor bleaching of the pIRIR signal would be a severe problem. However, no signs of soil reworking were visible in the soil profile at the depth of this sample, so this theory is rejected.

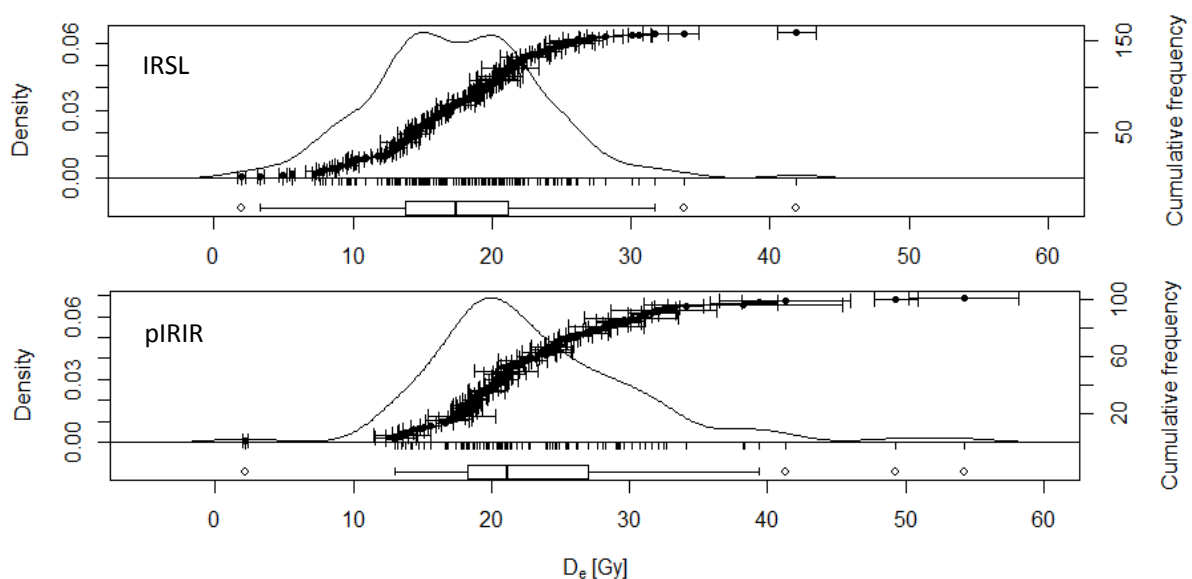


Figure 10 Equivalent dose distributions for both signals of sample NCL-1117122 (165 cm depth).

Another explanation for the wide IRSL distribution could be that the fading rate of the IRSL signal is less consistent over the total population of grains than for the pIRIR signal. This sample could contain grains fading at different rates. In that case, the bulk fading rate is not representative for each individual grain, because the fading rate of a grain depends on the rate at which a grain receives radiation from its environment (Wallinga et al. 2007). If the IRSL signal indeed consists of different grain populations fading at different rates, the pIRIR age is a better estimation of the burial age than the IRSL age. Since evidence is present for fading problems but not for bleaching problems, the pIRIR signal was considered most suitable for age calculation. If bleaching problems are small or absent for a cover sand sample they are also expected to be small or absent for the samples in the reworking zone, because reworking is assumed to be a better bleaching process than cover sand deposition. In the reworking process grains are constantly and very intensively mixed and therefore they have more bleaching possibilities than cover sand grains that are deposited in one single, relatively short event. Another reason why the pIRIR signal is preferred over the IRSL signal is that the ages of the samples taken in undisturbed cover sand parent material, which is known to be deposited at the end of the Pleistocene, correspond well to this expected age. The fading corrected IRSL ages of this cover sand sample were only 9.7 ka (weighted mean) and 9.8 ka (MAM), whereas the fading corrected ages of the pIRIR signal were 11.2 ka (weighted mean) and 12.3 ka (MAM). The expected Pleistocene age of cover sand (Zeeberg 1998) is around 11-12 ka, so the pIRIR weighted mean is more consistent with chronostratigraphic evidence regarding the timing of cover sand activity.

After selection of the most appropriate signal, the most appropriate age model was selected. For some samples, the conventional logged minimum age model could not be applied because of negative dose measurements for individual grains. For these samples, the unlogged model had to be applied. This resulted in a mixture of ages determined with the logged and unlogged age model. The ages older than around 350 years that were calculated with the unlogged model were underestimated compared to the ages calculated with the logged model, resulting in local age inversions. For sample NCL-1117133 the age was negative within the standard error (Appendix Table 7). Moreover, visual inspection of radial plots and D_e distributions showed that the 2σ iterated weighted mean generally resulted in equally good or better estimations of the minimum age peak than the minimum age model (see the radial plots and D_e distributions in the Appendix). For these reasons, the iterated weighted mean age was deemed more appropriate for age estimation.

The weighted mean age of sample NCL-1117123 (see pIRIR radial plot for this sample in the Appendix), for which only a few measurements fall inside the 2σ bar, remains problematic. The weighted mean is clearly an underestimation. However, the MAM seems to overestimate the age of the leading-edge D_e population. The cause of these problems might be that the youngest grains in this sample do not form a leading-edge peak in the distribution of this sample, but rather a plateau joining to the left side of the main peak of undisturbed grains (see pIRIR D_e distribution for this sample in the Appendix).

Considering these arguments, the pIRIR iterated weighted mean age was chosen as best representative of the leading-edge D_e population. The age-depth profile for this age seems to be divided in two parts (Figure 11) with distinctly different age-depth gradients. In the upper part the age increases with depth at a rate of 0.0087 ka/cm, whereas the age increases with 0.25 ka/cm in the lower part. The boundary between the upper and lower part lies as a depth of approximately 120 cm. This division of the profile in two parts could be caused by high accumulation rates and high soil reworking rates in the upper part, related to plaggic agriculture. This hypothesis is supported by the fact that all layers in the upper part have been ploughed (Figure 8 and Table 1). The reworking rates and accumulation rates are discussed in the following sections.

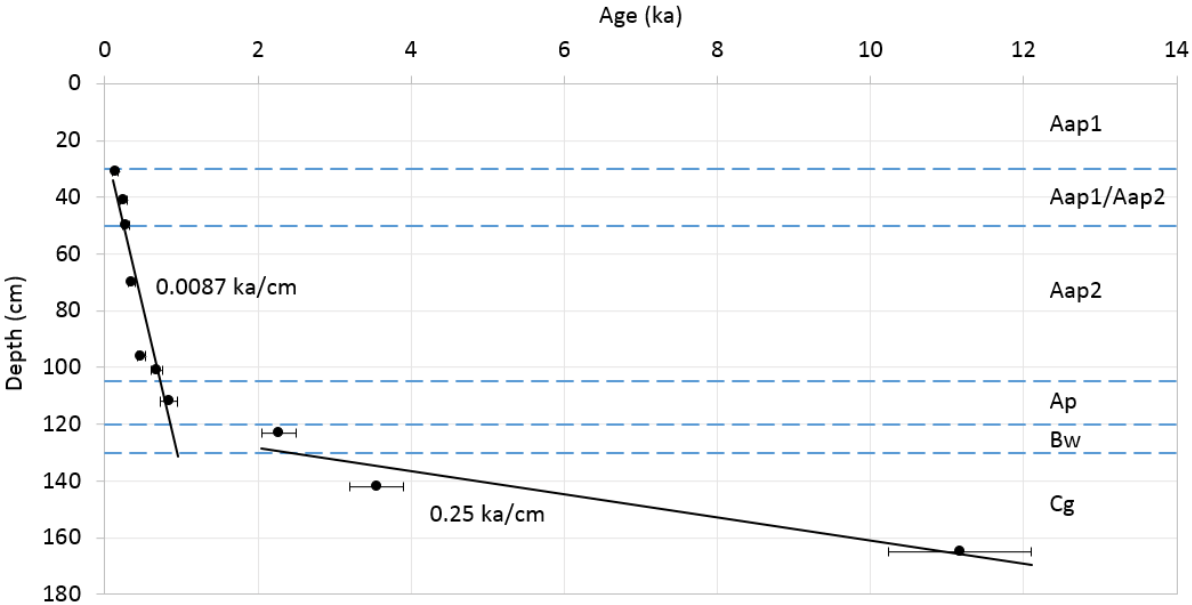


Figure 11 Age-depth profile with gradients for the upper (<120 cm) and lower (>120 cm) part of the profile.

Soil reworking rates

Effective soil reworking rates were determined for all samples according to the method proposed by Reimann et al. (2017). They calculated reworking rates for a situation in which saturated feldspar grains derived from weathered bedrock were present. These grains had never been exposed to daylight and as a consequence they were never bleached, so their luminescence signal was infinitely large. In this study no saturated grains are present, but the applied principle is the same. The method by Reimann et al. (2017) can be generalised to other situations when the terms ‘unsaturated’ and ‘saturated’ are replaced by the terms ‘reworked’ and ‘unreworked’ respectively. The non-saturation factor is then replaced by a reworking intensity factor (RIF) that indicates the fraction of reworked grains in a sample. This means that the RIF needs to be determined for both the reworked and unreworked samples, because even in samples that are mostly undisturbed, a few percent of grains might be reworked by bioturbation. In this study, the cover sand aged grains represent the unreworked fraction and all younger grains form the reworked fraction. In determining the RIF, a distinction was made between the upper (<120 cm) and lower (>120 cm) part of the soil profile. Soil reworking in the upper part of the profile is the result of both biological and anthropogenic reworking, where the influence of the latter is assumed to dominate because ploughing is a much more intensive mixing process than bioturbation. The lower part of the profile has never been ploughed and mixing is exclusively the result of bioturbation. For the lower part of the soil profile the RIF depends on the fraction of cover sand aged grains present in the sample. The cover sand aged grains were separated from the reworked grains using the finite mixture model by Galbraith (2005). The function *calc_FiniteMixture* in the R package *Luminescence* was applied to the equivalent dose datasets trying 2 to 10 components. In all three cases, the 2-component model resulted in the lowest BIC-value and was therefore the best fit to the data (Schwarz 1978). The youngest component was assumed to represent the reworked grains and the fraction of this component of the total sample was used as the RIF. The finite mixture model could not be applied to the samples in the upper part of the profile, because of the presence of negative equivalent dose measurements. The RIF in the upper part is assumed to be 1, because the historical practice of stepwise application of a thin plaggic layer and ploughing can be assumed to fully bleach every single-grain. This assumption appears to be a reasonable approximation, because the three RIF values that could be calculated were 0.96 for the samples NCL-1117127 and NCL-1117131 and 0.89 for sample NCL-1117132. For this latter sample application of the finite mixture model results in three components, of which only the first one is considered to be cover sand. The dose of the middle component is 3.55 ± 1.02 Gy and therefore much too young to be included in the cover sand fraction. The presence of a few cover sand aged grains in this part of the profile is considered sample contamination or upward movement of older grains. As expected, the soil reworking rates were indeed higher in the upper part of the profile than in the lower part (Figure 12, Appendix Table 8). The difference is one to two orders of magnitude. The rates in the upper part of the profile are showing only a very small increase with depth, whereas the lower three samples are different from the upper part and their reworking rates rapidly decrease with depth.

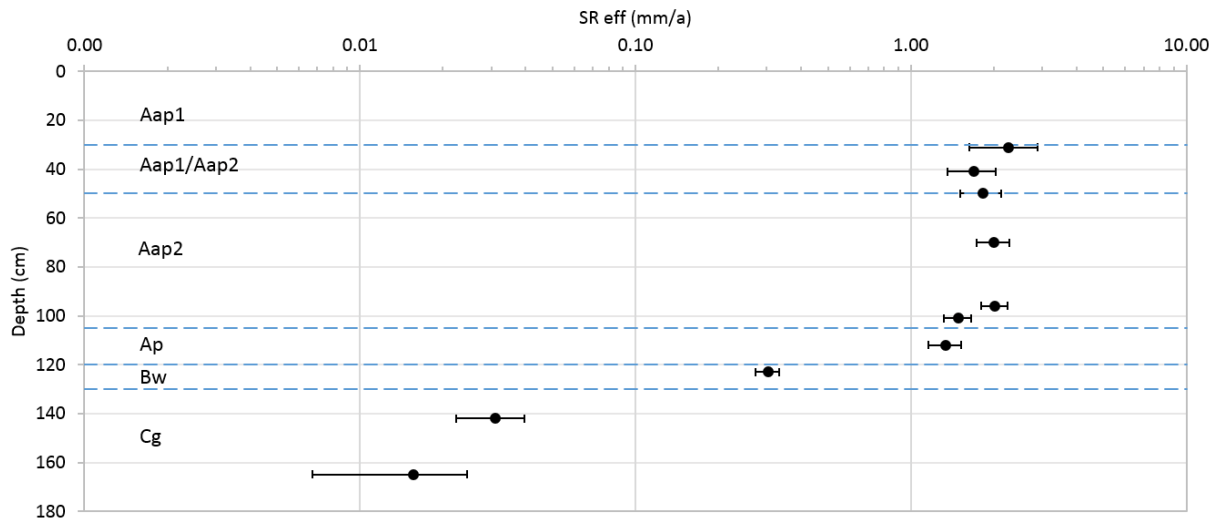


Figure 12 Effective soil reworking rates for all samples. Note that the horizontal axis is drawn on a 10-log scale.

Plaggen accumulation rates

The simplest way to calculate accumulation rates is to divide the depth difference between two samples by their difference in burial age. In plaggic soils however, the burial dose has been completely removed from the grains because of bleaching by intensive mixing. Therefore, the accumulation rate cannot be calculated directly and is estimated by the rate of upward movement of the ploughing depth. These rates are equal when the ploughing depth is assumed to have a constant value over the entire history of this soil. A value of 25 cm was used for the ploughing depth. Because the luminescence signal of a grain is constantly reset during ploughing, the signal only starts to build up when the grain is buried below the ploughing horizon. The age of a sample then gives the time that has passed since this sample was buried below the ploughing depth. The calculation of the accumulation rate is explained using sample NCL-1117131 at the depth of 50 cm as an example (Figure 13).

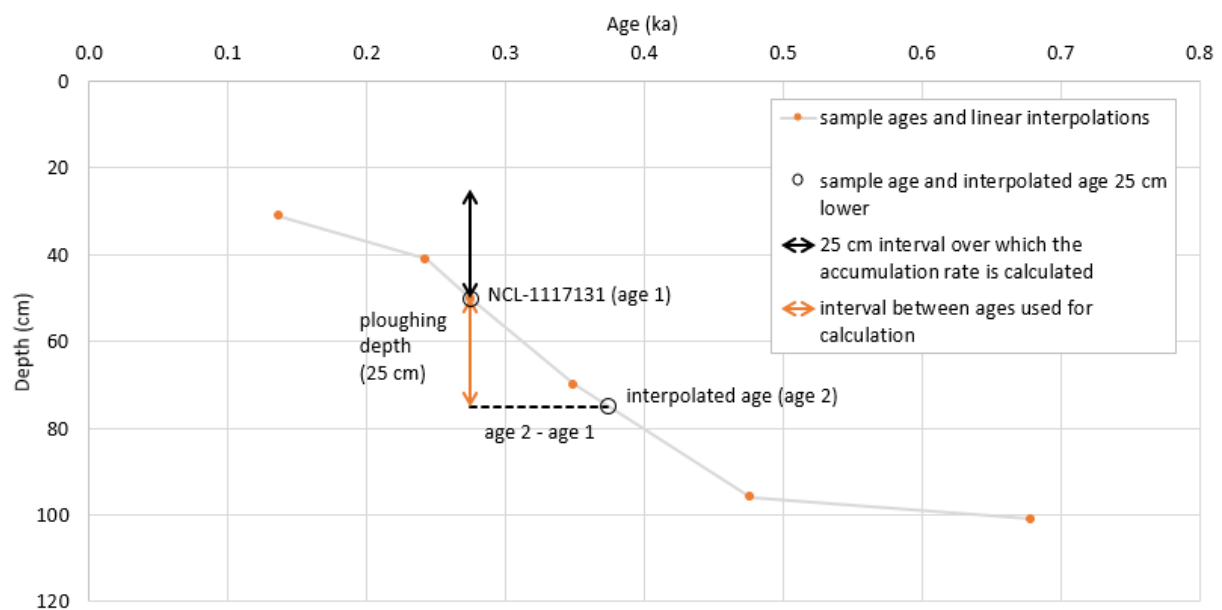


Figure 13 Calculation of the accumulation rate. In this example the calculation interval is equal to the ploughing depth.

The age of this sample (age 1) is the time that has passed since this sample was buried below the ploughing horizon. Age 2 is the time that has passed since an 'interpolated sample' at 25 cm below sample NCL-1117131 was buried below the ploughing horizon. The difference between these ages is the time that it took for the bottom of the ploughed layer to get from 75 cm to 50 cm in the present-time soil profile as a result of plaggen accumulation. Over the same time interval that the bottom of the ploughing depth moved 25 cm upward, the surface of the soil accumulated over the 25 cm interval above the sample. In summary, the accumulation rate over an interval above a sample is calculated as:

$$\text{accumulation rate} = \frac{\text{depth of age 1} - \text{depth of age 2}}{\text{age 2} - \text{age 1}}$$

The age of the ‘interpolated sample’ is calculated as the linearly interpolated age between the samples directly above and below that point. It is essential that the point at the lower end of the calculation interval is still inside the plaggic deposits, so above a depth of 105 cm. This ensures that the calculated rate is indeed purely an accumulation rate of plaggic deposits. Using this restriction, the accumulation rates in the 25 cm above the upper four samples could be calculated and also the accumulation rate in the 5 cm above sample NCL-1117127 (Table 4). If the depth interval for the accumulation rate was spread over two horizons, the dominant horizon was used for interpretation. The accumulation rate is low in the Aap1 horizon, high in the Aap1/Aap2 transition horizon and intermediate in the Aap2 horizon, but there is no clear difference between ages within the standard error. A more elaborate version of Table 4 that includes the ages used for calculation of the accumulation rate is included in Table 9 in the Appendix.

Table 4 Accumulation rates in the plaggic horizons of the sampled soil profile.

Depth interval (cm below surface)	Horizon	Accumulation rate (mm/a)
6 - 31	Aap1	1.56 ± 0.63
16 - 41	Aap1/Aap2	2.74 ± 2.02
25 - 50	Aap1/Aap2	2.53 ± 1.71
45 - 70	Aap2	2.04 ± 1.17
66 - 71	Aap2	2.04 ± 6.28

It is important to note that accumulation rates do not have to be calculated for an interval size equal to the ploughing depth. The interval size can also be smaller or larger. Neither is it necessary that one of the ages is a known sample age. The accumulation rate can also be calculated with two interpolated ages, but of course this will increase the uncertainty of the results. However, the calculated accumulation rate always applies to an interval of the size of the ploughing depth higher up in the soil profile than the interval between the ages used in the calculation. Figure 14 shows how the accumulation rate should be calculated for generalised situations when the calculation interval is smaller or larger than the ploughing depth.

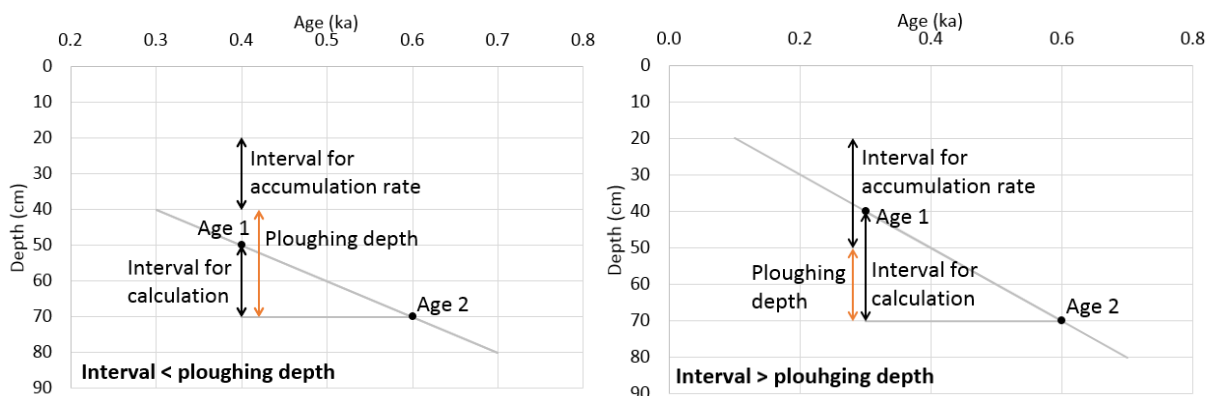


Figure 14 Calculation of the accumulation rate when the calculation interval is not equal to the ploughing depth.

Discussion and interpretation

Feldspar single-grain dating of plaggic soils in context

This is the first application of feldspar single-grain luminescence dating to a plaggic anthrosol. This method has shown to produce a chronologically consistent age-depth profile. Ages increase systematically with depth and the expected end-Pleistocene age (Zeeberg 1998) of cover sand sample NCL-1117122 is well reflected by the pIRIR iterated weighted mean age of 11.2 ± 0.9 ka determined for that sample. The feldspar single-grain ages in the profile are in line with independent age estimates determined by Smeenge (in preparation) using the well-established multiple grain quartz luminescence dating method. An elaboration was made on the applications of the effective soil reworking rate as developed by Reimann et al. (2017). Apart from situations in which saturated grains from weathered bedrock are present in a reworked soil, the effective reworking rate can also be calculated for purely sedimentary situations. This enabled quantification of the mixing processes in a plaggic soil and it clearly showed the difference between natural and anthropogenic reworking. For the first time historical accumulation rates in plaggic deposits have been calculated using luminescence dating. These rates are useful for the reconstruction of former management practices and possibly they are useful as well for improvement of modern agricultural techniques.

This shows the potential of single-grain feldspar luminescence dating for future dating applications. Its results are very promising and although less feldspar than quartz is generally present in a sample, the great advantage of feldspar is that much more grains emit a suitable luminescence signal. This makes feldspar a very efficient mineral for luminescence dating and in particular for single-grain luminescence dating. Because the quartz multiple grain ages by Smeenge (in preparation) were used to correct the feldspar ages for poor bleaching, the feldspar ages determined here cannot be directly compared to these quartz ages. To be able to compare the ages, a modern surface sample exposed to natural daylight (modern analogue) should have been used to correct for poor bleaching. A real sample or an extrapolated sample could have been used for this. The luminescence signal in such a sample is a good estimate of the age inheritance due to incomplete signal resetting. In fact, such a correction would be better even if ages were not to be compared because the poor bleaching correction using quartz ages has an important shortcoming. The quartz ages used for correction have been linearly interpolated to depth because the quartz samples and feldspar samples were taken at different depths. Since plaggen application is a gradual process and since the soil is constantly reworked during this process, the age increase with depth between two subsequent samples can indeed be considered linear. However, the uncertainties of these quartz ages could not be interpolated. They were not included in the error-weighted mean age, which has now only been based on the error on the feldspar age.

Start of plaggic agriculture

To determine the moment at which plaggic agriculture started at the investigated location, the age below the lowest plaggic horizon should be used. This age reflects the moment when the non-plaggic soil was buried below the ploughing horizon as a result of the first plaggen addition. Sample NCL-1117125 in the Ap horizon is the first sample below the Aap2 horizon. It has an age of 839 ± 113 a, which indicates that plaggic agriculture started around 1178 ± 113 AD. This age is probably slightly underestimated so that plaggic agriculture started to develop a little earlier. The reason for underestimation is that the age is based on an error-weighted mean equivalent dose. The errors of the D_e estimates of individual grains serve as a weighting factor with the more precise values getting a

higher weight. Since lower values generally have a lower absolute error, they have more effect on the weighted mean than higher values. Galbraith and Roberts (2012) have observed the same for the unlogged common age model, which is similar to the iterated weighted mean used here. When standard errors of the D_e increase with increasing D_e value, the unlogged version of the common age model may be biased towards the lower D_e values in a distribution, resulting in an age underestimation. If the minimum age model would have been used instead of the weighted mean the same problem would occur, because for the pIRIR signal of sample NCL-1117125 the unlogged common age model had to be used. According to Arnold et al. (2009) the unlogged minimum age model gives accurate burial doses and luminescence ages for samples younger than 350 a. For samples older than 350 a the age is underestimated when using the unlogged minimum age model. Therefore, the pIRIR unlogged MAM age of 627 ± 145 a for sample NCL-1117125 is an underestimation as well, and even more severely than the weighted mean age.

Taking this underestimation into account, plaggic agriculture probably started a little earlier around the beginning of the High Middle Ages (1000-1300 AD). In this subperiod of the Middle Ages the European population increased and new areas of land were cultivated for agriculture (Bartlett 1994). Knowledge on crops and agriculture expanded and better ploughing techniques were developed. The start of plaggic agriculture as determined by feldspar single grain luminescence dating is consistent with these historical events. The start of plaggic agriculture also coincides with the Medieval Warm Period (950-1250 AD). The Medieval Warm Period was described by Lamb (1965) as a period in which temperature changes of 1.2 to 1.4 °C and an annual rainfall increase of 10 % occurred in England. These warmer and more humid conditions increased the number of crop types that could be grown. In combination with improved agricultural techniques and increased food demand related to population growth this led to a higher agricultural intensity and presumably also to the start of plaggic agriculture at the sampled location.

Natural and anthropogenic soil reworking

The rates in the upper part of the soil profile are the combined rates of natural and anthropogenic reworking, whereas the rates in the lower part of the profile are purely natural. The soil reworking rates increase suddenly at the boundary between those two parts. The reason for this sudden increase could be that the upper part of the natural (non-plaggic) profile is not preserved. Soil reworking in this part was probably of intermediate intensity, given the presence of a non-plaggic ploughing layer. For the upper part of the profile, the effects of bioturbation and anthropogenic reworking cannot be separated. Bioturbation is probably larger in the upper part than in the lower part, because the high organic matter content in plaggic deposits leads to the presence of more soil fauna. Although bioturbation can be expected to be larger in the upper part than in the lower part, the effect of ploughing on the reworking rate is expected to dominate here. The natural effective reworking rates in the lower part of the profile are 0.02 ± 0.01 mm/a, 0.03 ± 0.01 mm/a and 0.30 ± 0.03 mm/a (Appendix Table 8). Comparable (apparent) rates of 0.1 to 0.5 mm/a and 0.03 to 0.2 mm/a were found by Stockmann et al. (2013). These rates were determined in the upper 50 cm under a forest, so these rates are also based on exclusively natural reworking. Reimann et al. (2017) found effective soil reworking rates up to 0.067 ± 0.010 mm/a for a hillslope in Spain where mixing was only caused by natural processes. This similarity in reworking rates with other natural reworking rates suggests that natural soil reworking at shallow depths happens at a fairly constant rate, independent of the natural circumstances. The effective reworking rates in the ploughed part of the profile are between 1.34 ± 0.18 mm/a and 2.26 ± 0.63 mm/a (Appendix Table 8). As expected, these rates are much higher than the natural rates as a result of ploughing. This confirms

the initial hypothesis that anthropogenic reworking is dominant over natural reworking in the upper part of the soil profile.

Some remarks should be made on the calculation of the reworking rates. The minimum overdispersion σ_b was used as input for the finite mixture model. The overdispersion of the cover sand component will indeed be close to σ_b , because the sample that was used to derive it (NCL-1117122) fully consists of unmixed cover sand. However, the finite mixture model assumes that the overdispersion is the same for all components, so in this case the overdispersion used for the reworked (mainly plaggenic) subpopulation will be equal to the overdispersion of the cover sand subpopulation. These two components cannot be assumed to have equal overdispersion, because plaggen deposition occurs slowly at a rate of about 1-2 mm/a while cover sand deposition is an instantaneous event. Therefore, the overdispersion for perfectly bleached cover sand will be lower than for perfectly bleached plaggen deposits and the value of σ_b will underestimate the overdispersion of the reworked fraction. In the finite mixture model all fitted dose distributions depend on each other, because their proportions must add up to one. Underestimation of the overdispersion of the reworking peak may therefore cause overestimation of the number of components and erroneous mixing proportions (Galbraith and Roberts 2012). The mean value and proportion (and as a consequence the RIF) of the cover sand peak then partially depend on the other fitted distributions and this would lead to a wrong age estimation. Another disadvantage of the finite mixture model is that the R function *calc_FiniteMixture* does not consider the uncertainty of σ_b . This leads to extra uncertainty in the proportions and mean values of all components.

Instead of using the finite mixture model, the cover sand grains could be separated from the reworked grains with the maximum age model. This model calculates one single age that represents the boundary between cover sand and reworked grains, namely the peak of the cover sand subpopulation. The advantage is that this model calculates the mean value of the cover sand peak independently of the other peaks. However, the uncertainty of σ_b is not taken into account by the R function *calc_MaxDose* either and, more importantly, the lower half of the cover sand peak would be incorporated in the proportion of reworked grains. The finite mixture model does not use a rigid age boundary between the reworked grains and cover sand grains. Whereas the maximum age model does not consider the uncertainties of the boundary age and the individual D_e values, the finite mixture model does consider all these uncertainties. This leads to a much more reliable estimate of the proportions of cover sand grains and reworked grains in a sample, so the finite mixture model was preferred over the maximum age model.

Historical accumulation of plaggen

Based on the accumulation rates obtained for this location, historical plaggen accumulation seems to be divided in three phases. In the first phase the Aap2 horizon was formed at a seemingly constant rate of 2.04 mm/a (two values of 2.04 ± 1.17 mm/a and 2.04 ± 6.28 mm/a were measured). The second phase is characterised by more rapid accumulation rates in the Aap1/Aap2 horizon of 2.53 ± 1.71 mm/a and 2.74 ± 2.02 mm/a. Above this transition horizon the accumulation rate appears to be lower with a value of 1.56 ± 0.63 mm/a. This marks the third accumulation phase related to the formation of the Aap1 horizon. Within one standard error the accumulation rates do not differ a lot between the three phases, so the division in three phases should be considered with some caution. As discussed earlier, the first phase of plaggen accumulation starts at the beginning of the High Middle Ages. The European population was already growing, but not as fast as in later stages. Probably the development of

agricultural techniques was still in a beginning phase as well, so the soil was not yet used very intensively. Together these factors will have led to the relatively low accumulation rate in the first phase. In the Aap1/Aap2 horizon (phase 2) ages between 137 and 275 years were found. This means that this layer was still ploughed long after the end of the Middle Ages. Because the population was growing and because the ploughing techniques were improving, it is probable that this transition horizon started to accumulate in the High Middle Ages. That is also the period in which rapid plaggen accumulation would be expected based on the need for food and the favourable climatic conditions for agriculture. It is also possible that the soil was abandoned for some time between phase one and two, which could explain why the accumulation rate increases suddenly with about 25% instead of gradually. The Aap1 horizon above sample NCL-1117133, which has an age of 137 ± 37 a, was formed in the third and last phase of plaggen accumulation. It can be assumed that this layer is older than indicated by this sample, because the age only gives the time of latest reworking. A part of this layer may have accumulated in the Middle Ages, which could explain the still rather high value of the accumulation rate. High accumulation rates were found for a period extending far beyond the Middle Ages into the late 19th century. This leads to the conclusion that plaggen were applied from the High Middle Ages until the late 19th century. This is supported by Blume and Leinweber (2004) who investigated plaggic agriculture in Denmark, NW Germany, Belgium and the Netherlands and concluded that it existed until last century. After that the plaggen addition probably slowed down. Presently, the location is not used for agricultural purposes any more.

It was assumed that the ploughing layer had a constant depth of 25 cm throughout the history of this plaggic soil. This value was used because the ploughing depth has probably increased over time from about 20 cm in the Middle Ages to 30 cm after the Middle Ages. The assumption of a constant ploughing depth might lead to wrong values of the accumulation rate in the upper and lower parts of the plaggic deposits, where the historical ploughing depth deviated from 25 cm. To quantify this effect, the accumulation rates were also calculated for ploughing depths of 20 and 30 cm (Table 5). More elaborate tables that include the ages used for calculation of the accumulation rates are included in Table 9, Table 10 and Table 11 in the Appendix. For a ploughing depth of 20 cm the accumulation rate for the upper interval could not be calculated because the upper age needed for calculation was above the upper age measured, so no age interpolation could be made.

Table 5 Accumulation rates for ploughing depths of 20 and 30 cm. The accumulation rates for a ploughing depth of 25 cm are shown again for comparison. These accumulation rates are calculated over the same intervals as in Table 4. Ploughing depth is abbreviated to pd.

Depth interval (cm below surface)	Accumulation rates (mm/a)		
	pd = 20 cm	pd = 25 cm	pd = 30 cm
6 - 31	--	1.56 ± 0.63	1.99 ± 1.20
16 - 41	1.99 ± 1.20	2.74 ± 2.02	2.68 ± 2.17
25 - 50	2.72 ± 2.13	2.53 ± 1.71	2.39 ± 1.66
45 - 70	2.14 ± 1.36	2.04 ± 1.17	0.94 ± 0.36
66 - 71	2.04 ± 6.67	2.04 ± 6.28	0.25 ± 0.19

For the lower part of the soil profile, the accumulation rates calculated with a ploughing depth of 20 cm are probably closest to the real historical accumulation rates. Their values are a little higher than for a ploughing depth of 25 cm, but the difference is very small compared to the standard errors. For the upper part of the profile, the accumulation rates calculated using a ploughing depth of 30 cm are probably a better estimate. Here the difference between 25 cm and 30 is again smaller than the

standard errors, so the assumption of a ploughing depth of 25 cm seems to be appropriate for the whole profile. If instead the ploughing depth was varied from 20 cm to 30 cm, the general interpretation of the three phases of accumulation would still be valid, though the differences between the phases would be smaller. A striking effect occurs when a ploughing depth of 30 cm is applied for the lower part of the soil profile. The calculated accumulation rates are very low and precise. The low value is the result of the large age-depth gradient between the points that were used to derive the accumulation rate (Table 11). The accumulation rates are also very precise as a consequence of the same large age-depth gradient and of the low values of the accumulation rates themselves, because both factors are included in the error calculation.

Conclusions

Single-grain feldspar luminescence dating was used to derive ages at several depths inside a plaggic anthrosol. Analysis of the soil profile showed that at this location plaggic agriculture first appeared around the beginning of the High Middle Ages (1000-1300 AD). At this time the European population started to grow and agricultural techniques improved. The appearance of plaggic agriculture can also be linked to the Medieval Warm Period (950-1250 AD), in which elevated temperature and humidity increased agricultural possibilities. Plaggic agriculture thrived during this period, as can be derived from the rapid accumulation rates. After the Middle Ages, plaggen accumulation slowed down and the soil at the sampling location was not ploughed any more. Effective soil reworking rates at several depths in the soil profile revealed the impact of human activity on soil mixing. The difference between natural soil reworking and reworking by ploughing has been quantified for the first time using feldspar single-grain luminescence dating. A substantial difference in reworking rate of one to two orders of magnitude between both mixing processes was found. The feldspar single-grain ages are all consistent with independent quartz multiple grain OSL age estimates derived from different samples taken at the same location. An important advantage of dating single feldspar grains over dating single quartz grains is that a much larger percentage of the feldspar grains emits a suitable luminescence signal. This property combined with the consistency of the ages with independent age estimates from a well-established method and with the dates of historical events shows the potential of this new method for future applications.

Acknowledgements

I would like to thank Harm Smeenge for letting me use the yet unpublished quartz luminescence ages of his PhD research. I also thank Mr. Borgerink for allowing me to take samples on his field, Erwin Steijsiger for his help during field work, Erna Voskuilen for teaching me all necessary lab skills, Alice Versendaal for her help with R and Matlab and of course both of my supervisors, Tony Reimann for his enthusiasm and the helpful discussions and Jakob Wallinga for his critical view on decisive moments throughout the process of this thesis.

References

AHN (2012). Interpolated AHN2 0.5 meter maaiveld raster, kaartblad 29cn2, Actueel Hoogtebestand Nederland: downloaded from pdok.nl on 14 July 2017.

Arnold, L. J., R. Bailey and G. Tucker (2007). "Statistical treatment of fluvial dose distributions from southern Colorado arroyo deposits." Quaternary Geochronology **2**(1): 162-167.

Arnold, L. J., R. G. Roberts, R. F. Galbraith and S. DeLong (2009). "A revised burial dose estimation procedure for optical dating of young and modern-age sediments." Quaternary Geochronology **4**(4): 306-325.

Bartlett, R. (1994). The making of Europe: conquest, colonization and cultural change 950-1350, Penguin UK.

Bateman, M. D., C. D. Frederick, M. K. Jaiswal and A. K. Singhvi (2003). "Investigations into the potential effects of pedoturbation on luminescence dating." Quaternary Science Reviews **22**(10): 1169-1176.

Behre, K.-E. (2000). "Fruhe Ackersysteme, Dungemethoden und die Entstehung der nordwestdeutschen Heiden." Archaeologisches Korrespondenzblatt **30**(1): 135-151.

Blume, H. P. and P. Leinweber (2004). "Plaggen soils: landscape history, properties, and classification." Journal of Plant Nutrition and Soil Science **167**(3): 319-327.

Bokhorst, M., G. Duller and J. Van Mourik (2005). "Optical dating of a Fimic Anthrosol in the southern Netherlands." Journal of Archaeological Science **32**(4): 547-553.

Castel, I., E. Koster and R. Slotboom (1989). "Morphogenetic aspects and age of Late Holocene eolian drift sands in Northwest Europe." Zeitschrift fur Geomorphologie **33**(1): 1-26.

Cordell, D., J.-O. Drangert and S. White (2009). "The story of phosphorus: global food security and food for thought." Global environmental change **19**(2): 292-305.

Cunningham, A. C. and J. Wallinga (2012). "Realizing the potential of fluvial archives using robust OSL chronologies." Quaternary Geochronology **12**: 98-106.

Demuro, M., L. J. Arnold, D. G. Froese and R. G. Roberts (2013). "OSL dating of loess deposits bracketing Sheep Creek tephra beds, northwest Canada: dim and problematic single-grain OSL characteristics and their effect on multi-grain age estimates." Quaternary Geochronology **15**: 67-87.

Dudal, R. and P. Driessen (1991). The major soils of the world: Lecture notes on their geography, formation, properties and use.

Duller, G. (2006). "Single grain optical dating of glacial deposits." Quaternary Geochronology **1**(4): 296-304.

Duller, G. (2015). "The Analyst software package for luminescence data: overview and recent improvements." Ancient TL **33**(1): 35-42.

Duller, G. A. (2008). "Single-grain optical dating of Quaternary sediments: why aliquot size matters in luminescence dating." Boreas **37**(4): 589-612.

Efron, B. and R. Tibshirani (1993). An Introduction to the Bootstrap New York, Chapman and Hall.

Fastabend, H. and F. von Raupach (1962). "Ergebnisse der C14-Untersuchungen an einigen Plaggenböden des Emslandes." Geol. Jb. **79**: 863-866.

Freibauer, A., M. D. Rounsevell, P. Smith and J. Verhagen (2004). "Carbon sequestration in the agricultural soils of Europe." Geoderma **122**(1): 1-23.

Galbraith, R. F. (2005). Statistics for fission track analysis, CRC Press.

Galbraith, R. F. and R. G. Roberts (2012). "Statistical aspects of equivalent dose and error calculation and display in OSL dating: an overview and some recommendations." Quaternary Geochronology **11**: 1-27.

Galbraith, R. F., R. G. Roberts, G. M. Laslett, H. Yoshida and J. M. Olley (1999). "Optical dating of single and multiple grains of quartz from Jinmium rock shelter, northern Australia: Part I, experimental design and statistical models." Archaeometry **41**(2): 339-364.

Giani, L., L. Makowsky and K. Mueller (2014). "Plaggic Anthrosol: Soil of the Year 2013 in Germany: An overview on its formation, distribution, classification, soil function and threats." Journal of Plant Nutrition and Soil Science **177**(3): 320-329.

Gliganic, L., J.-H. May and T. J. Cohen (2015). "All mixed up: Using single-grain equivalent dose distributions to identify phases of pedogenic mixing on a dryland alluvial fan." Quaternary International **362**: 23-33.

Gliganic, L. A., T. J. Cohen, M. Slack and J. K. Feathers (2016). "Sediment mixing in aeolian sandsheets identified and quantified using single-grain optically stimulated luminescence." Quaternary Geochronology **32**: 53-66.

Godfrey-Smith, D. I., D. J. Huntley and W.-H. Chen (1988). "Optical dating studies of quartz and feldspar sediment extracts." Quaternary Science Reviews **7**(3-4): 373-380.

Heimsath, A. M., J. Chappell, N. A. Spooner and D. G. Questiaux (2002). "Creeping soil." Geology **30**(2): 111-114.

Heineman, B. (1973). "Bodenkundliche Untersuchungen an einem Megalithgrab unter Plaggenesch in Osnabrück-Nahne." Nachr. Nieders. Urgesch. **42**: 211-219.

Hülle, D., A. Hilgers, P. Kühn and U. Radtke (2009). "The potential of optically stimulated luminescence for dating periglacial slope deposits—A case study from the Taunus area, Germany." Geomorphology **109**(1): 66-78.

Huntley, D. J. and M. Lamothe (2001). "Ubiquity of anomalous fading in K-feldspars and the measurement and correction for it in optical dating." Canadian Journal of Earth Sciences **38**(7): 1093-1106.

Jain, M. and C. Ankjærgaard (2011). "Towards a non-fading signal in feldspar: insight into charge transport and tunnelling from time-resolved optically stimulated luminescence." Radiation Measurements **46**(3): 292-309.

Jain, M., J.-P. Buylaert, K. J. Thomsen and A. S. Murray (2015). "Further investigations on 'non-fading' in K-Feldspar." Quaternary International **362**: 3-7.

Kars, R. H., T. Reimann, C. Ankjærgaard and J. Wallinga (2014). "Bleaching of the post-IR IRSL signal: new insights for feldspar luminescence dating." Boreas **43**(4): 780-791.

Kristensen, J. A., K. J. Thomsen, A. S. Murray, J.-P. Buylaert, M. Jain and H. Breuning-Madsen (2015). "Quantification of termite bioturbation in a savannah ecosystem: application of OSL dating." Quaternary Geochronology **30**: 334-341.

Lamb, H. H. (1965). "The early medieval warm epoch and its sequel." Palaeogeography, Palaeoclimatology, Palaeoecology **1**: 13-37.

Lukas, S., J. Q. Spencer, R. A. Robinson and D. I. Benn (2007). "Problems associated with luminescence dating of Late Quaternary glacial sediments in the NW Scottish Highlands." Quaternary Geochronology **2**(1): 243-248.

Lungershausen, U., A. Larsen, H.-R. Bork and R. Duttman (2017). "Anthropogenic influence on rates of aeolian dune activity within the northern European Sand Belt and socio-economic feedbacks over the last 2500 years." The Holocene: 0959683617715693.

Merante, P., C. Dibari, R. Ferrise, B. Sánchez, A. Iglesias, J. P. Lesschen, P. Kuikman, J. Yeluripati, P. Smith and M. Bindi (2017). "Adopting soil organic carbon management practices in soils of varying quality: Implications and perspectives in Europe." Soil and Tillage Research **165**: 95-106.

Mucher, H., R. Slotboom and W. Ten Veen (1989). "Een enkeerdgrond palynologisch ontsloten; toepassing van de palynologie bij de toetsing van en de aanvulling op archivalische data." Geografisch Tijdschrift **23**: 109-118.

Murray, A. and R. Roberts (1998). "Measurement of the equivalent dose in quartz using a regenerative-dose single-aliquot protocol." Radiation Measurements **29**(5): 503-515.

Murray, A., K. J. Thomsen, N. Masuda, J.-P. Buylaert and M. Jain (2012). "Identifying well-bleached quartz using the different bleaching rates of quartz and feldspar luminescence signals." Radiation Measurements **47**(9): 688-695.

Niemeier, G. and W. Taschenmacher (1939). "Plaggenböden. Beiträge zu ihrer genetik und typologie." Westfälische Forschungen **2**: 29-64.

Olley, J. M., R. G. Roberts and A. S. Murray (1997). "Disequilibria in the uranium decay series in sedimentary deposits at Allen's Cave, Nullarbor Plain, Australia: implications for dose rate determinations." Radiation Measurements **27**(2): 433-443.

Pape, J. (1970). "Plaggen soils in the Netherlands." Geoderma **4**(3): 229-255.

Pietsch, T. J., J. M. Olley and G. C. Nanson (2008). "Fluvial transport as a natural luminescence sensitiser of quartz." Quaternary Geochronology **3**(4): 365-376.

Prescott, J. R. and J. T. Hutton (1994). "Cosmic ray contributions to dose rates for luminescence and ESR dating: large depths and long-term time variations." Radiation Measurements **23**(2-3): 497-500.

Preusser, F., D. Degering, M. Fuchs, A. Hilgers, A. Kadereit, N. Klasen, M. Krbetschek, D. Richter and J. Q. Spencer (2008). "Luminescence dating: basics, methods and applications." Quaternary Science Journal **57**(1-2): 95-149.

Reimann, T., A. Román-Sánchez, T. Vanwalleghem and J. Wallinga (2017). "Getting a grip on soil reworking-Single-grain feldspar luminescence as a novel tool to quantify soil reworking rates." Quaternary Geochronology.

Reimann, T., K. J. Thomsen, M. Jain, A. S. Murray and M. Frechen (2012). "Single-grain dating of young sediments using the pIRIR signal from feldspar." Quaternary Geochronology **11**: 28-41.

Reimann, T., S. Tsukamoto, M. Naumann and M. Frechen (2011). "The potential of using K-rich feldspars for optical dating of young coastal sediments—a test case from Darss-Zingst peninsula (southern Baltic Sea coast)." Quaternary Geochronology **6**(2): 207-222.

Sandvik, B. (2009). Shapefile of the Netherlands: downloaded from thematicmapping.org on 14 July 2017.

Sawakuchi, A. O., C. Guedes, R. DeWitt, P. C. F. Giannini, M. Blair, D. Nascimento and F. Faleiros (2012). "Quartz OSL sensitivity as a proxy for storm activity on the southern Brazilian coast during the Late Holocene." Quaternary Geochronology **13**: 92-102.

Schwarz, G. (1978). "Estimating the dimensions of a model." The annals of statistics **6**(2): 461-464.

Smedley, R., G. Duller, N. Pearce and H. Roberts (2012). "Determining the K-content of single-grains of feldspar for luminescence dating." Radiation Measurements **47**(9): 790-796.

Smeenge, H. (in preparation). PhD Thesis.

Spek, T. (2004). Het Drentse esdorpenlandschap; een historisch-geografische studie.

Spooner, N. A. (1994). "The anomalous fading of infrared-stimulated luminescence from feldspars." Radiation Measurements **23**(2-3): 625-632.

Stockmann, U., B. Minasny, T. Pietsch and A. McBratney (2013). "Quantifying processes of pedogenesis using optically stimulated luminescence." European Journal of Soil Science **64**(1): 145-160.

Thomsen, K. J., A. S. Murray, M. Jain and L. Bøtter-Jensen (2008). "Laboratory fading rates of various luminescence signals from feldspar-rich sediment extracts." Radiation Measurements **43**(9-10): 1474-1486.

Van Mourik, J., A. Seijmonsbergen, R. Slotboom and J. Wallinga (2012). "Impact of human land use on soils and landforms in cultural landscapes on aeolian sandy substrates (Maashorst, SE-Netherlands)." Quaternary International **265**: 74-89.

Van Mourik, J., R. Slotboom and J. Wallinga (2011). "Chronology of plaggic deposits; palynology, radiocarbon and optically stimulated luminescence dating of the Posteles (NE-Netherlands)." Catena **84**(1): 54-60.

Van Mourik, J., P. Wartenbergh, W. Mook and H. Streurman (1995). "Radiocarbon dating of paleosols in aeolian sands." Mededelingen Rijks Geologische Dienst **52**.

Wallinga, J., A. J. Bos, P. Dorenbos, A. S. Murray and J. Schokker (2007). "A test case for anomalous fading correction in IRSL dating." Quaternary Geochronology **2**(1): 216-221.

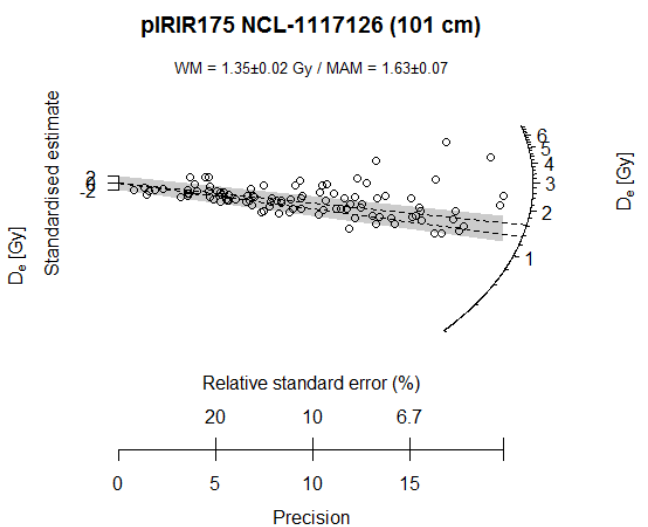
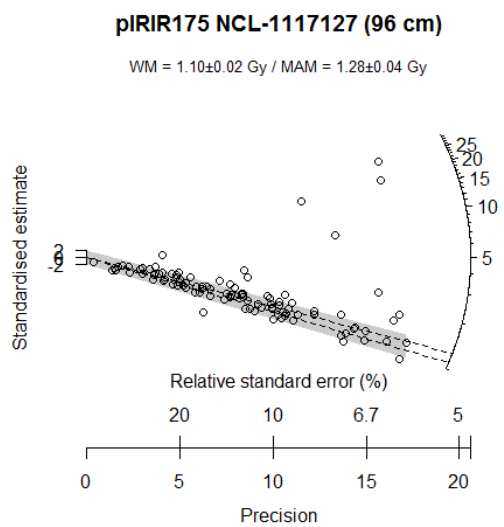
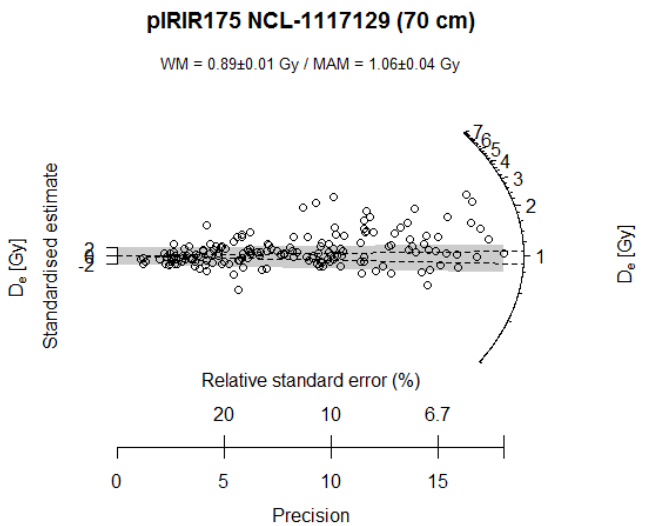
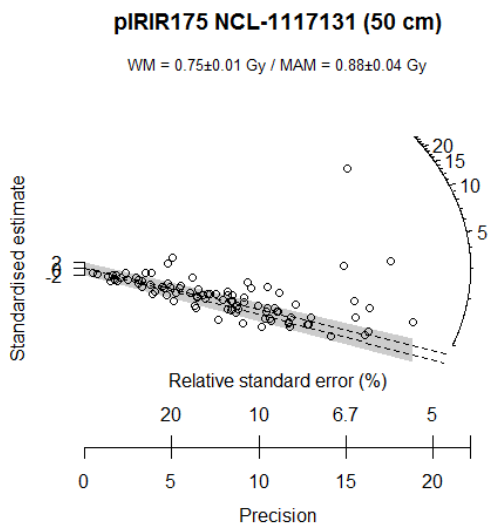
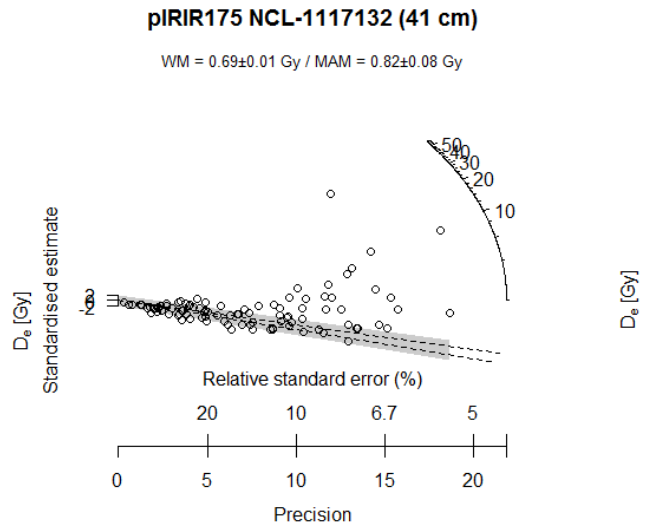
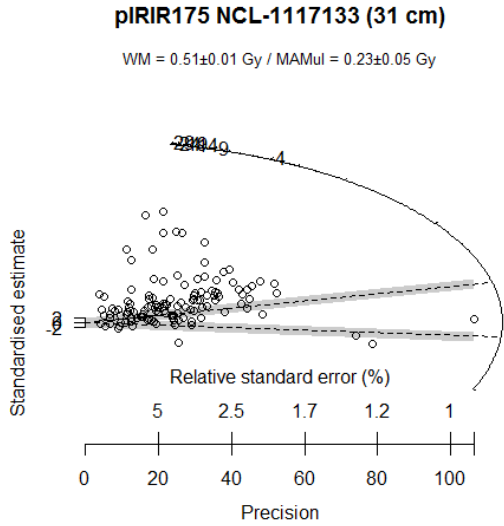
Wilkinson, M. T., P. J. Richards and G. S. Humphreys (2009). "Breaking ground: pedological, geological, and ecological implications of soil bioturbation." Earth-Science Reviews **97**(1): 257-272.

Zeeberg, J. (1998). "The European sand belt in eastern Europe and comparison of Late Glacial dune orientation with GCM simulation results." Boreas **27**(2): 127-139.

Appendix

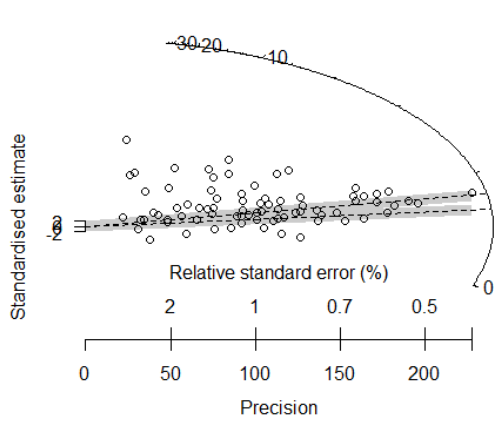
pIRIR sample descriptions

Radial plots



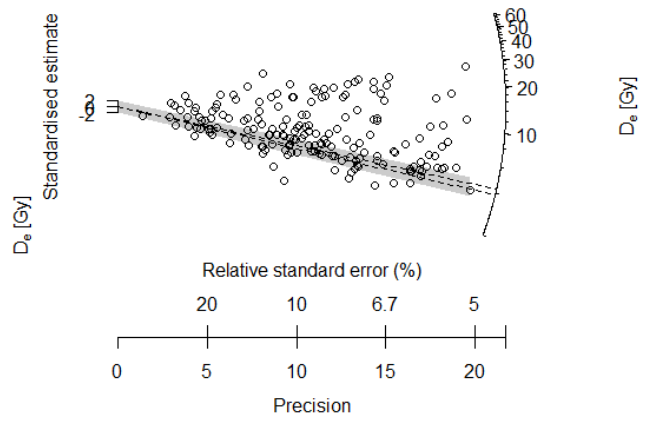
PIRIR175 NCL-1117125 (112 cm)

WM = 1.57 ± 0.02 Gy / MAMul = 1.31 ± 0.17 Gy



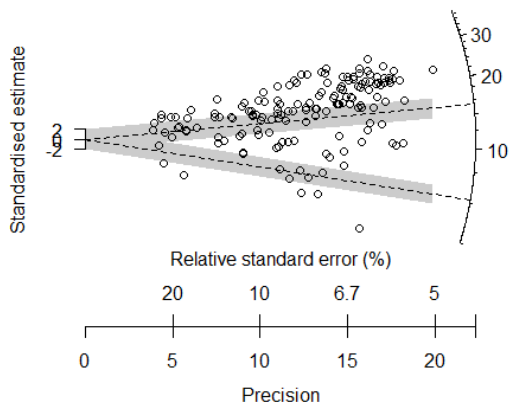
PIRIR175 NCL-1117124 (123 cm)

WM = 3.88 ± 0.04 Gy / MAM = 4.31 ± 0.26 Gy



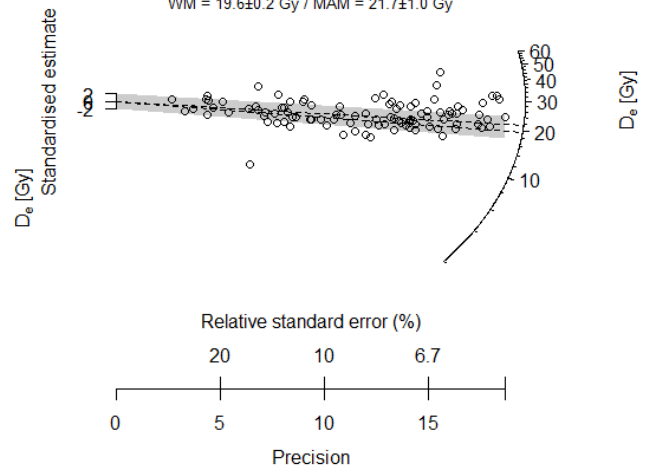
PIRIR175 NCL-1117123 (142 cm)

WM = 6.2 ± 0.1 Gy / MAM = 15.2 ± 1.8 Gy

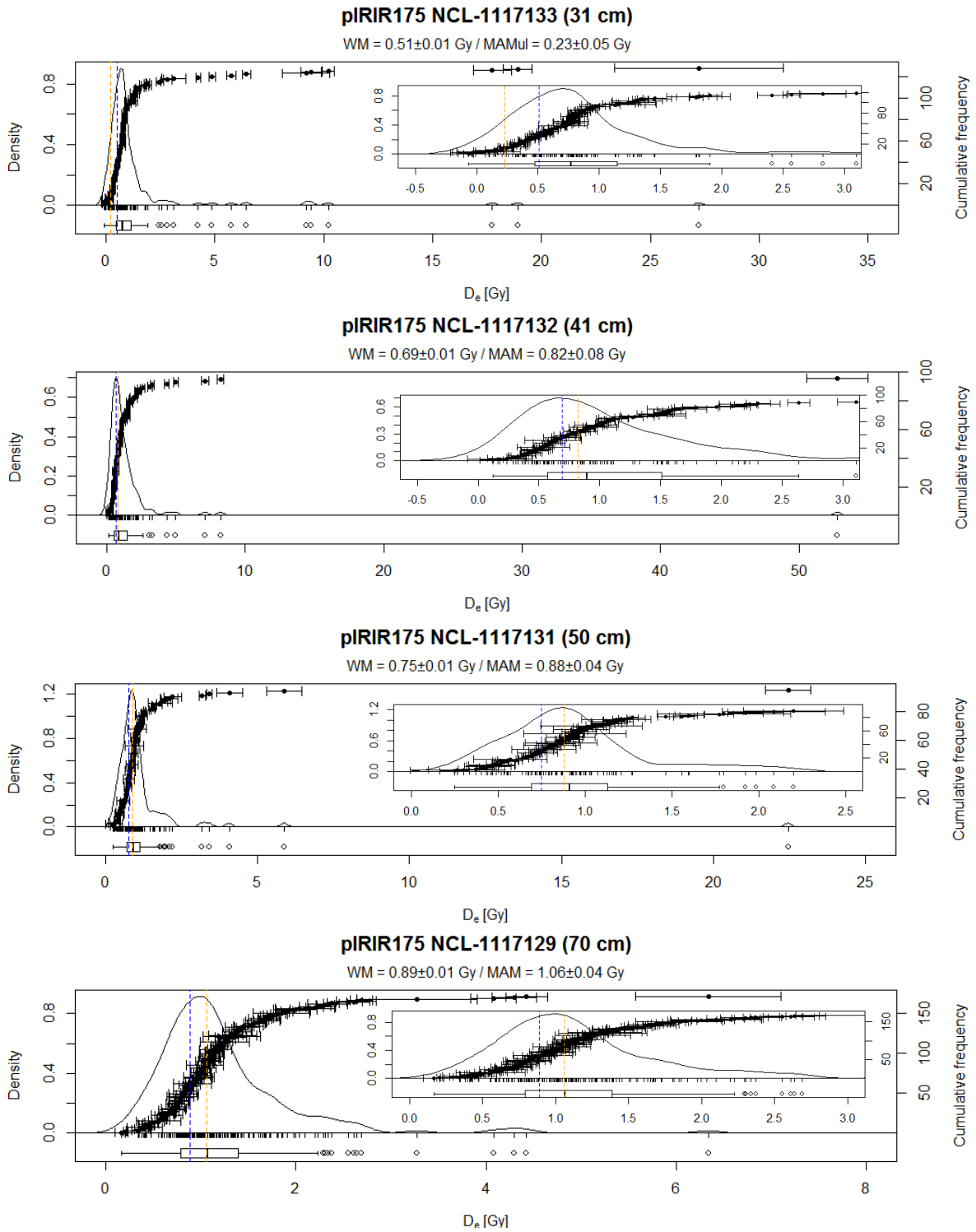


PIRIR175 NCL-1117122 (165 cm)

WM = 19.6 ± 0.2 Gy / MAM = 21.7 ± 1.0 Gy

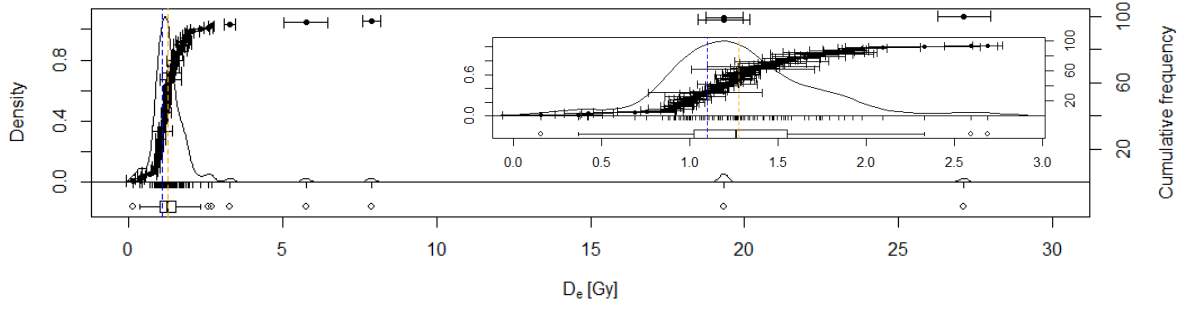


Equivalent dose distributions (with inset plots of the leading-edge population)



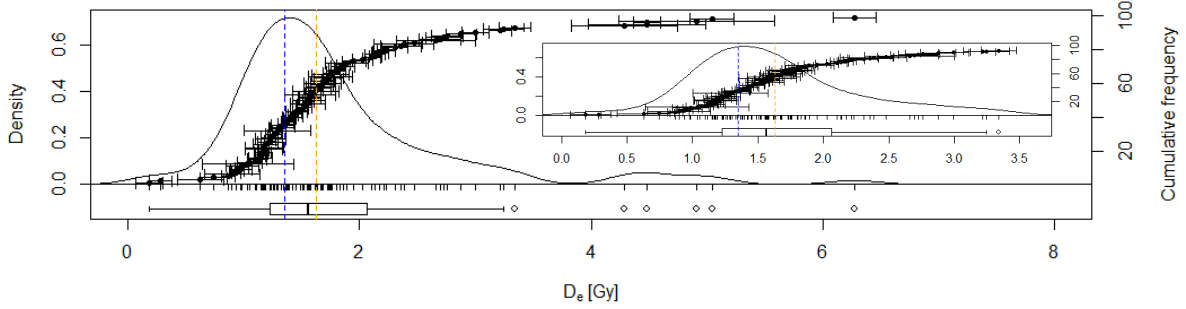
pIRIR175 NCL-1117127 (96 cm)

WM = 1.10 ± 0.02 Gy / MAM = 1.28 ± 0.04 Gy



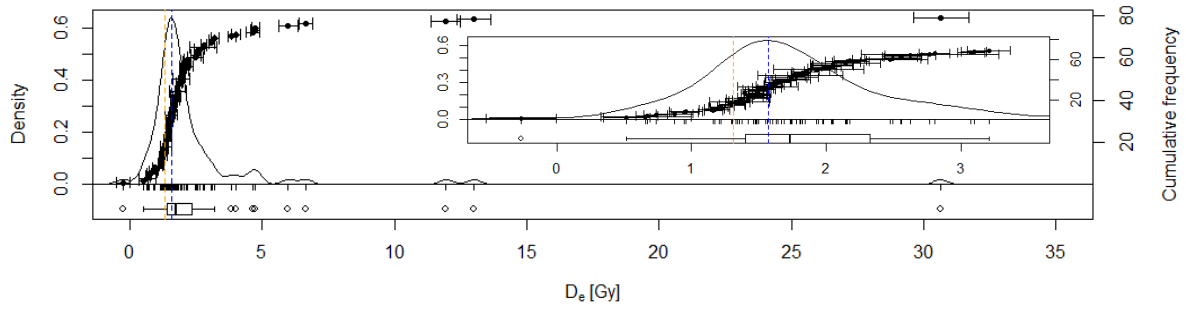
pIRIR175 NCL-1117126 (101 cm)

WM = 1.35 ± 0.02 Gy / MAM = 1.63 ± 0.07 Gy



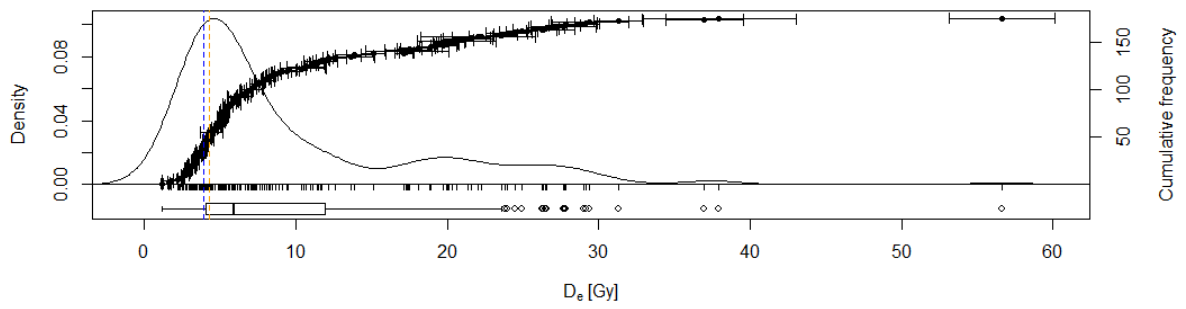
pIRIR175 NCL-1117125 (112 cm)

WM = 1.57 ± 0.02 Gy / MAMul = 1.31 ± 0.17 Gy



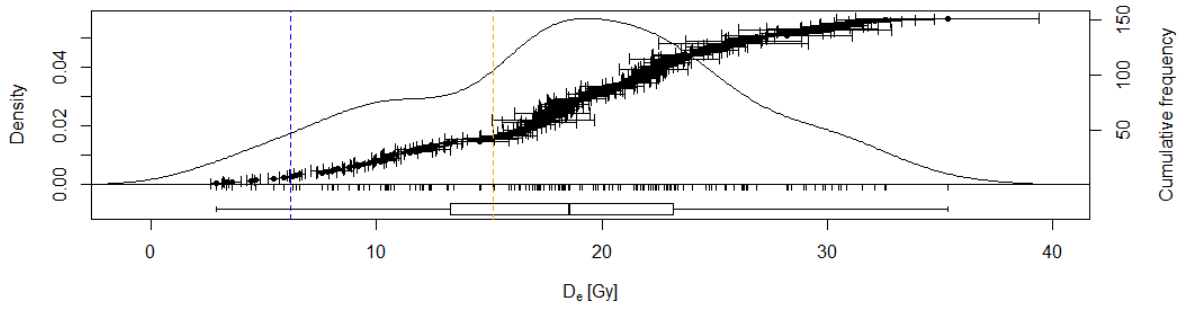
pIRIR175 NCL-1117124 (123 cm)

WM = 3.88 ± 0.04 Gy / MAM = 4.31 ± 0.26 Gy



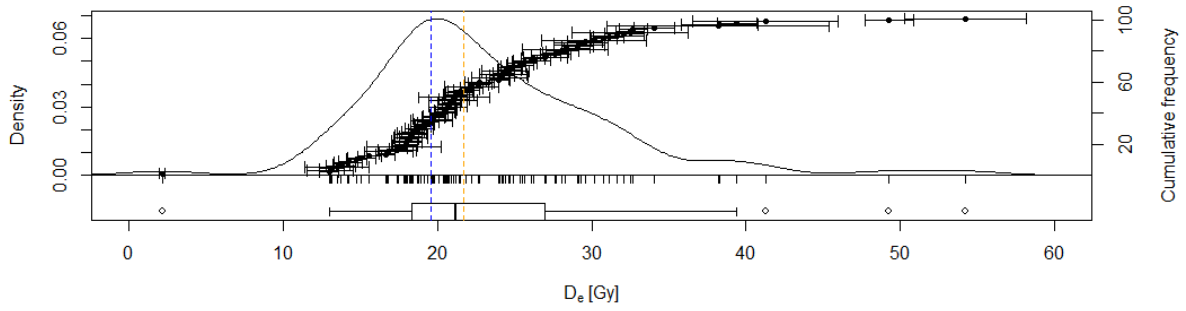
pIRIR175 NCL-1117123 (142 cm)

WM = 6.2 ± 0.1 Gy / MAM = 15.2 ± 1.8 Gy



pIRIR175 NCL-1117122 (165 cm)

WM = 19.6 ± 0.2 Gy / MAM = 21.7 ± 1.0 Gy

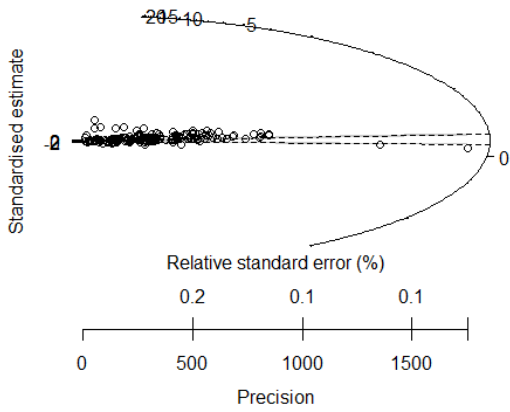


IRSL sample descriptions

Radial plots

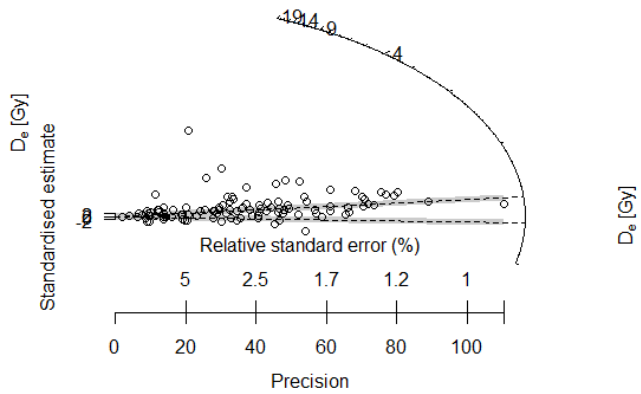
IRSL50 NCL-1117133 (31 cm)

WM = 0.30 ± 0.00 Gy / MAMul = 0.16 ± 0.04 Gy



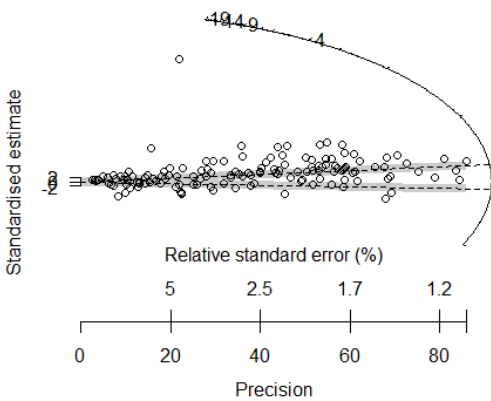
IRSL50 NCL-1117132 (41 cm)

WM = 0.45 ± 0.01 Gy / MAMul = 0.26 ± 0.04 Gy



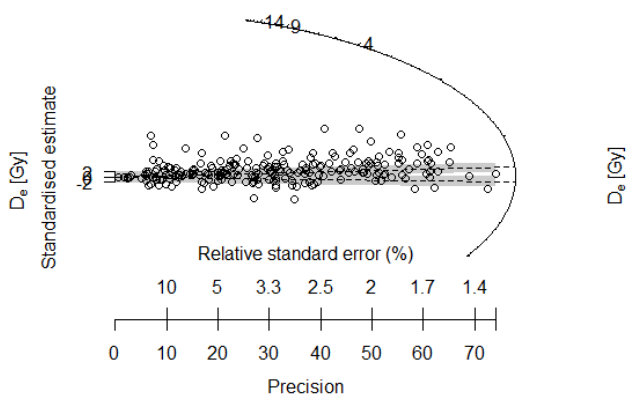
IRSL50 NCL-1117131 (50 cm)

WM = 0.53 ± 0.01 Gy / MAMul = 0.35 ± 0.04 Gy



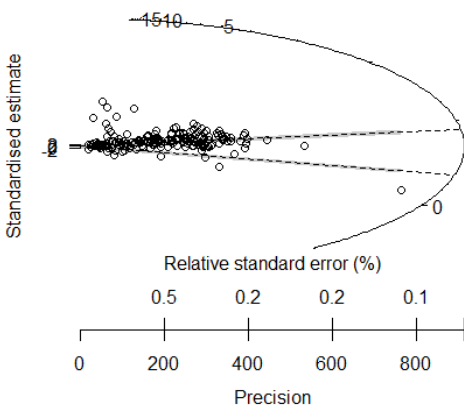
IRSL50 NCL-1117129 (70 cm)

WM = 0.69 ± 0.01 Gy / MAMul = 0.56 ± 0.06 Gy



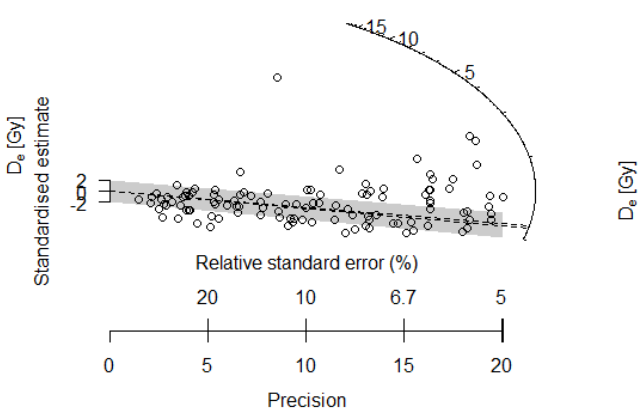
IRSL50 NCL-1117127 (96 cm)

WM = 0.89 ± 0.01 Gy / MAMul = 0.38 ± 0.16 Gy



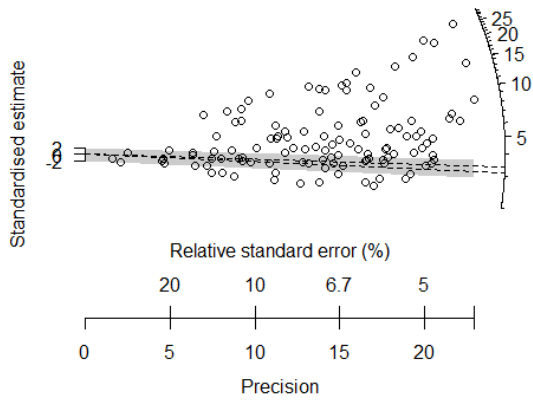
IRSL50 NCL-1117126 (101 cm)

WM = 1.10 ± 0.01 Gy / MAMul = 1.12 ± 0.07 Gy



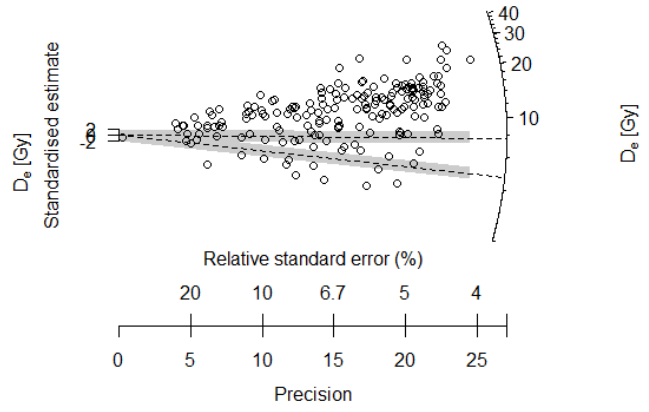
IRSL50 NCL-1117124 (123 cm)

WM = 3.16 ± 0.03 Gy / MAM = 3.41 ± 0.32 Gy



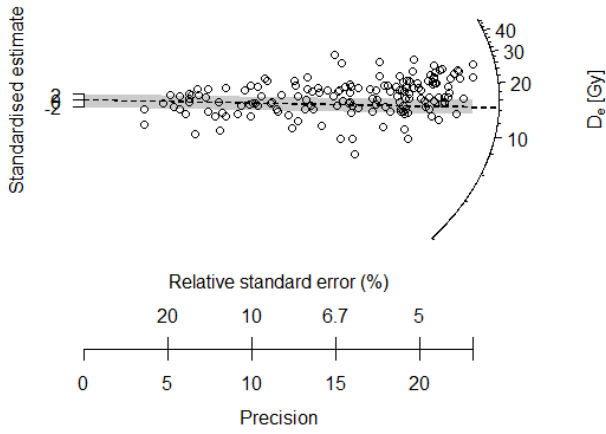
IRSL50 NCL-1117123 (142 cm)

WM = 4.7 ± 0.1 Gy / MAM = 7.7 ± 1.2 Gy

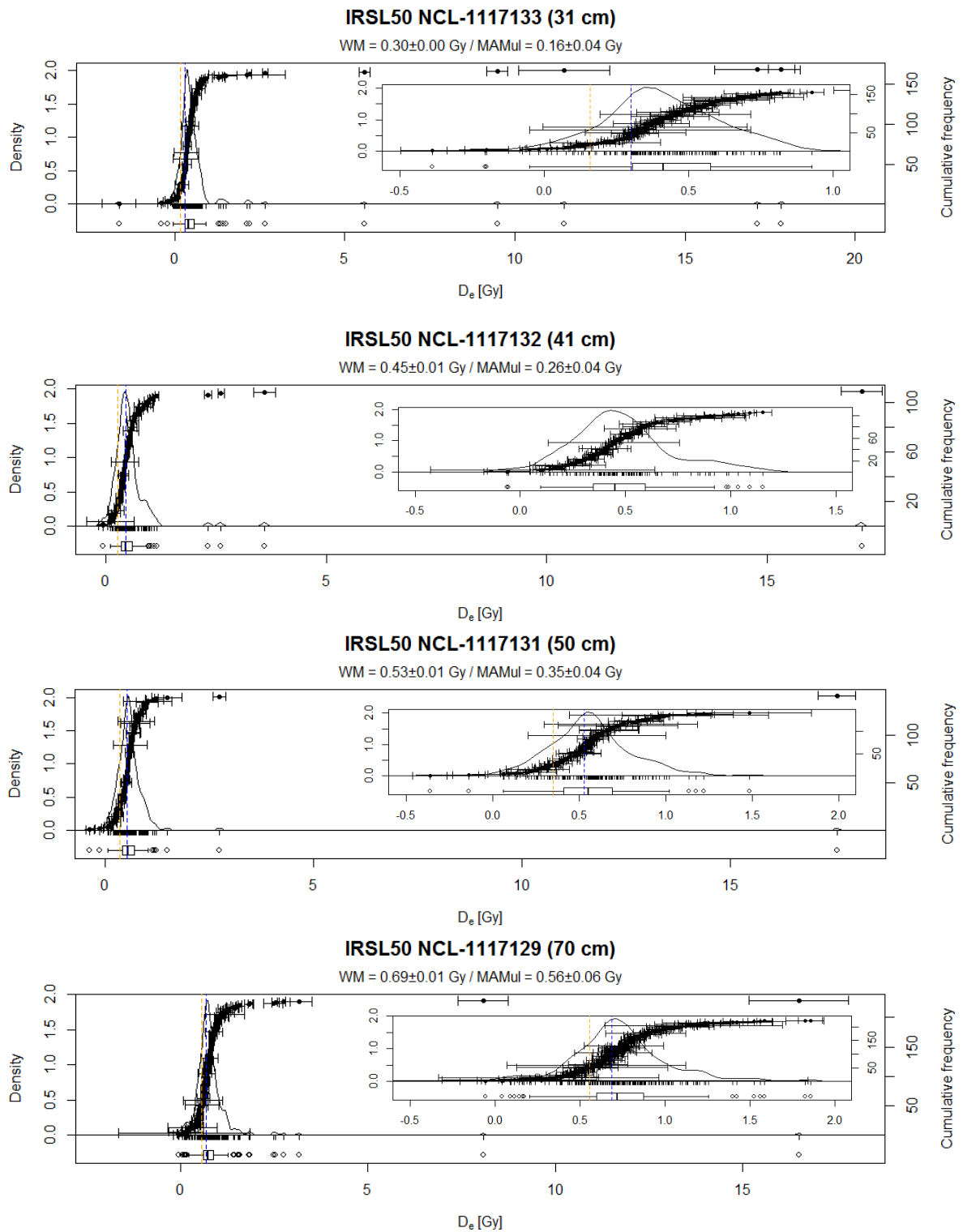


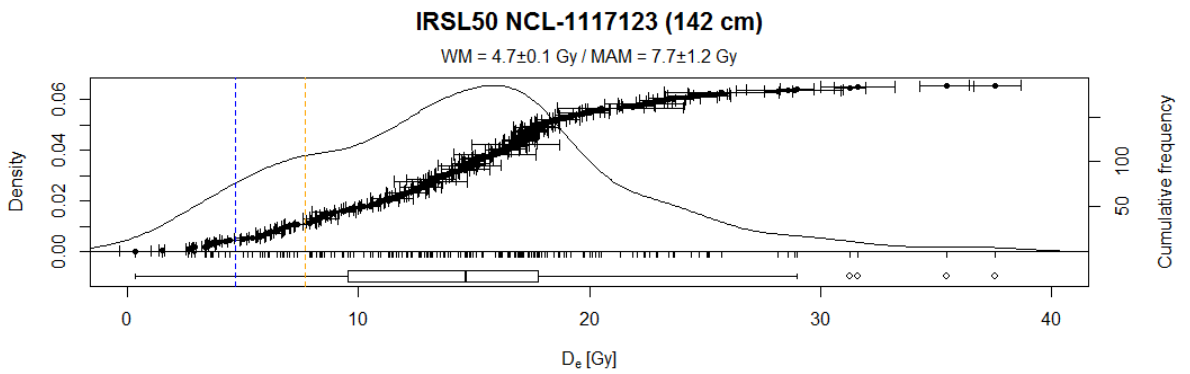
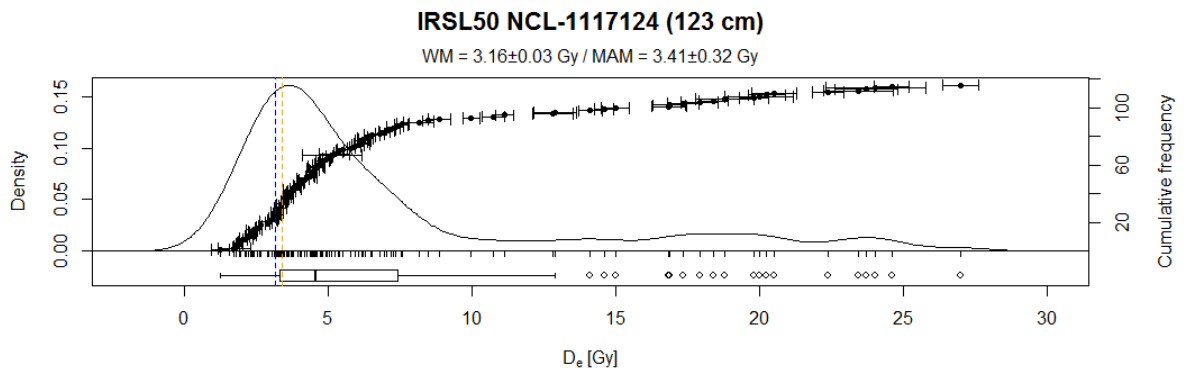
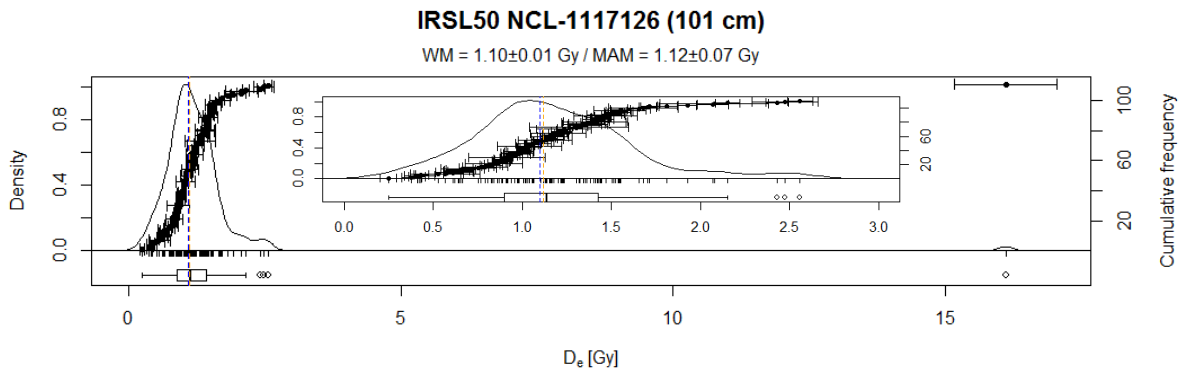
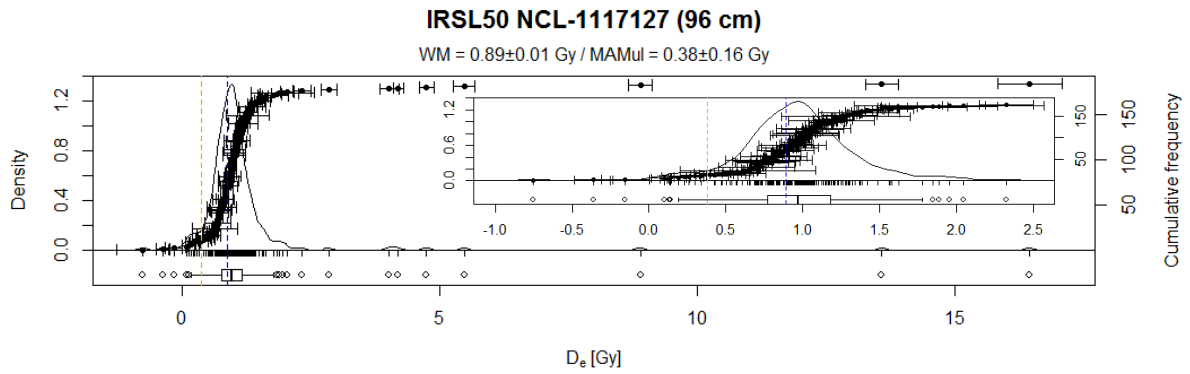
IRSL50 NCL-1117122 (165 cm)

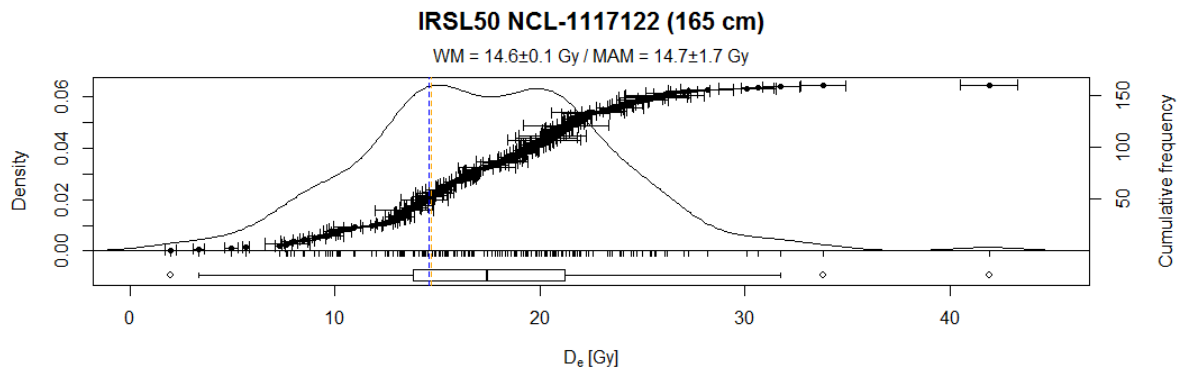
WM = 14.6 ± 0.1 Gy / MAM = 14.7 ± 1.7 Gy



Equivalent dose distributions (with inset plots of the leading-edge population)







Result tables

Overdispersion

Table 6 Overdispersion per sample for both signals

Sample	Depth (cm)	pIRIR overdispersion (%)	IRSL overdispersion (%)
NCL-1117133	31	32.9 ± 7.7	36.9 ± 3.9
NCL-1117132	41	46.2 ± 3.7	53.7 ± 3.6
NCL-1117131	50	74.4 ± 3.3	69.3 ± 4.6
NCL-1117129	70	39.6 ± 4.1	39.7 ± 8.5
NCL-1117127	96	39.0 ± 4.3	53.0 ± 9.7
NCL-1117126	101	58.8 ± 12.8	28.8 ± 2.7
NCL-1117125	112	44.7 ± 3.6	--
NCL-1117124	123	54.0 ± 10.0	34.4 ± 3.5
NCL-1117123	142	76.9 ± 12.5	42.9 ± 4.9
NCL-1117122	165	59.8 ± 6.2	53.2 ± 4.9

Ages

Table 7 Weighted mean and MAM-3 ages for the pIRIR and IRSL signal. Ages calculated with the unlogged MAM-3 are marked with a *.

Sample	Depth (cm)	pIRIR weighted mean age (ka)	pIRIR MAM-3 age (ka)	IRSL weighted mean age (ka)	IRSL MAM-3 age (ka)
NCL-1117133	31	0.14 ± 0.04	-0.08 ± 0.07 *	0.12 ± 0.03	0.14 ± 0.03 *
NCL-1117132	41	0.24 ± 0.05	0.29 ± 0.07	0.23 ± 0.03	0.21 ± 0.03 *
NCL-1117131	50	0.27 ± 0.05	0.31 ± 0.06	0.27 ± 0.04	0.26 ± 0.04 *
NCL-1117129	70	0.35 ± 0.05	0.40 ± 0.07	0.37 ± 0.04	0.40 ± 0.05 *
NCL-1117127	96	0.48 ± 0.05	0.54 ± 0.08	0.51 ± 0.06	0.28 ± 0.12 *
NCL-1117126	101	0.68 ± 0.08	0.82 ± 0.11	0.70 ± 0.08	0.83 ± 0.10
NCL-1117125	112	0.84 ± 0.11	0.63 ± 0.14 *	--	--
NCL-1117124	123	2.3 ± 0.2	2.5 ± 0.3	2.2 ± 0.2	2.5 ± 0.3
NCL-1117123	142	3.6 ± 0.4	9.0 ± 1.5	3.1 ± 0.3	5.4 ± 1.0
NCL-1117122	165	11.2 ± 0.9	12.3 ± 1.1	9.7 ± 0.8	9.8 ± 1.5

Soil reworking rates

Table 8 Soil reworking rates based on the pIRIR weighted mean age.

Sample	Depth (cm)	Soil reworking rate (mm/a)
NCL-1117133	31	2.26 ± 0.63
NCL-1117132	41	1.69 ± 0.34
NCL-1117131	50	1.82 ± 0.31
NCL-1117129	70	2.01 ± 0.27
NCL-1117127	96	2.01 ± 0.22
NCL-1117126	101	1.49 ± 0.17
NCL-1117125	112	1.34 ± 0.18
NCL-1117124	123	0.30 ± 0.03
NCL-1117123	142	0.03 ± 0.01
NCL-1117122	165	0.02 ± 0.01

Plaggen accumulation rates

Table 9 Plaggen accumulation rates based on the pIRIR weighted mean age and a ploughing depth of 25 cm.

Depth interval (cm)	Horizon	Lower interval end for calculation		Upper interval end for calculation		Accumulation rate (mm/a)
		Age (ka)	Depth (cm)	Age (ka)	Depth (cm)	
6 - 31	Aap1	0.30 ± 0.05	56	0.14 ± 0.04	31	1.56 ± 0.63
16 - 41	Aap1/Aap2	0.33 ± 0.05	66	0.24 ± 0.05	41	2.74 ± 2.02
25 - 50	Aap1/Aap2	0.37 ± 0.05	75	0.27 ± 0.05	50	2.53 ± 1.71
45 - 70	Aap2	0.47 ± 0.05	95	0.35 ± 0.05	70	2.04 ± 1.17
66 - 71	Aap2	0.48 ± 0.05	96	0.45 ± 0.05	91	2.04 ± 6.28

Table 10 Plaggen accumulation rates based on the pIRIR weighted mean age and a ploughing depth of 20 cm.

Depth interval (cm)	Horizon	Lower interval end for calculation		Upper interval end for calculation		Accumulation rate (mm/a)
		Age (ka)	Depth (cm)	Age (ka)	Depth (cm)	
6 - 31	Aap1	0.28 ± 0.05	51	--	26	--
16 - 41	Aap1/Aap2	0.32 ± 0.05	61	0.19 ± 0.05	36	1.99 ± 1.20
25 - 50	Aap1/Aap2	0.35 ± 0.05	70	0.26 ± 0.05	45	2.72 ± 2.13
45 - 70	Aap2	0.45 ± 0.05	90	0.33 ± 0.05	65	2.14 ± 1.36
66 - 71	Aap2	0.45 ± 0.05	91	0.43 ± 0.06	86	2.04 ± 6.67

Table 11 Plaggen accumulation rates based on the pIRIR weighted mean age and a ploughing depth of 30 cm.

Depth interval (cm)	Horizon	Lower interval end for calculation		Upper interval end for calculation		Accumulation rate (mm/a)
		Age (ka)	Depth (cm)	Age (ka)	Depth (cm)	
6 - 31	Aap1	0.32 ± 0.05	61	0.19 ± 0.05	36	1.99 ± 1.20
16 - 41	Aap1/Aap2	0.35 ± 0.05	71	0.26 ± 0.06	46	2.68 ± 2.17
25 - 50	Aap1/Aap2	0.40 ± 0.05	80	0.29 ± 0.05	55	2.39 ± 1.66
45 - 70	Aap2	0.64 ± 0.08	100	0.37 ± 0.05	75	0.94 ± 0.36
66 - 71	Aap2	0.68 ± 0.08	101	0.48 ± 0.05	96	0.25 ± 0.19